EVALUATING A NOVEL APPROACH FOR LOCATING PREFERENTIAL VAPOR TRANSPORT PATHWAYS IN THE VADOSE ZONE – JOINT-INTERPRETATION OF SOFT DATA FROM ELECTRICAL RESISTIVITY TOMOGRAPHY WITH HARD DATA

by

Luke Shannon

ABSTRACT

Volatilization of organic compounds and the radioactive decay of naturally occurring elements such as radium produce vapor plumes in the subsurface that can migrate horizontally and vertically throughout the unsaturated zone. Mass transfer of potentially harmful compounds can occur through these subsurface vapor transport pathways, resulting in the migration of contaminants into overlying buildings, reducing indoor air quality. This process is known as vapor intrusion (VI). Experimental investigations have shown that the evolution of VI pathways can be affected by surface events such as precipitation or irrigation, which can create wetting fronts that compress, displace, or restrict the flow of vapors in the subsurface.

I have developed a series of intermediate scale two-dimensional sand tank tests designed to investigate the complex interactions of soil moisture content and VI pathway evolution through a novel application of electrical resistivity tomography (ERT). The purpose of this study is to evaluate the performance of ERT in characterizing the moisture content and lithologic composition of the shallow subsurface, thus identifying potential VI pathways. I instrumented a sand tank with a network of moisture and temperature sensors and packed the tank in various heterogonous configurations with well-characterized fine and coarse sands. ERT data was collected along the surface profiles of the tank under various saturation conditions by controlling the water table elevation. Using a network of moisture and temperature sensors along with well-characterized laboratory sands, I was able to develop two-dimensional moisture and lithologic profiles based on hard data and compare against soft data collected using ERT.

The results from the ERT resistivity tests did not successfully characterize the relative soil moisture distributions or lithologic compositions in the physical VI tank models; however, all three sand tank configurations tested produced similar inaccuracies in the ERT inversion results which indicates the potential for a common source of error and therefore warrants further investigation. The similarities in the inversion inaccuracies show strong indications of model artifacts commonly associated with electrical sinks

present in a testing apparatus. Future studies will focus on addressing this electrical sink issue and retesting the final sand pack configuration using ERT.

After performing a series of two-dimensional ERT sand tank tests in the laboratory we upscaled the VI characterization methodology to perform a field demonstration of the characterization method. The goal in performing the ERT field demonstrations was to show how ERT could be used in a practical way to provide valuable qualitative information about VI pathways in the unsaturated zone. Evaluating the ERT field demonstration inversions over time provided a mechanism to spatially constrain a region of the subsurface where preferential VI pathways likely exist at the field demonstration site. This was accomplished by using ERT to capture time-series snap shots of a surface water infiltration event into horizontal sand channels and temporally matching the inversions to a continuously monitored VI signal entering the study site building.

By testing a series of well-designed research questions at intermediate-scales and at field-scales, I was able to demonstrate the practical applicability of the ERT VI characterization research performed for this thesis by investigating real-world environmental fate and transport problems such as VI. The ability of ERT to capture spatial and temporal information about the parameters that drive the evolution of VI pathways will aid future scientists and remediation site managers in developing better conceptual models of the processes controlling VI pathway evolution and in developing new screening methodologies used for site characterization of environmental fate and transport problems such as VI.

TABLE OF CONTENTS

LIST OF FIGURES

LIST OF TABLES

ACKNOWLEDGEMENTS

Funding for this study was made possible by a research grant from SERDP (*Project ER-1687*). All laboratory work was performed in the CESEP laboratory located at the CSM campus. The principal and co-investigators for this project were Tissa Illangasekare and Yaoguo Li. Brent Putman performed the geophysical inversions, as well as assisted in all field demonstrations. The field demonstrations were performed at a VI study site owned and operated by Professor Paul Johnson and his research group from ASU. Finally, Kathleen Smits provided critical guidance and oversight during all stages of laboratory investigation and field demonstration. I would like to thank all of above-mentioned parties for helping make this study come to fruition.

CHAPTER 1 – INTRODUCTION

Volatilization of organic compounds and the radioactive decay of naturally occurring radium produce vapor plumes in the subsurface that can migrate horizontally and vertically throughout the unsaturated zone. Based on the evolution of vapor transport pathways, vapor plumes can potentially migrate and infiltrate aquifers, causing significant groundwater contamination [*Baehr et al.*, 1999; *Christophersen et al.*, 2005], and into residential or commercial buildings through a process known as vapor intrusion (VI), often driving indoor air quality below minimum health standards [*Johnson and Ettinger*, 1991; *Hers et al.*, 2000; *Patterson and Davis*, 2009]. These subsurface vapor transport mechanisms create significant health concerns for the general public, which has been quantified in a recent study ranking VI of radon-decay products and the resulting inhalation risk as the second leading cause to lung cancer after smoking [*Darby et al.*, 2005].

Over the past two decades, several predictive models have been developed to quantify VI risk [*Jury et. al*, 1990; *Johnson and Ettinger*, 1991; *Mills et al.*, 2007; *Abreu and Johnson*, 2005, 2006; *Pennell et al.*, 2009]. Early versions of these models relied on relatively simple screening methods that incorporated either analytical or semi-analytical solutions based on one-dimensional steady state conditions [e.g. *Jury et. al*, 1990; *Johnson and Ettinger*, 1991] in homogeneous soils. These early models, however, made assumptions that greatly over simplified real world subsurface compositions [*Hers et al.*, 2002]. More recent three-dimensional models, such as those developed by *Abreu and Johnson* [2005] and *Pennell et al.* [2009], have made large advances in predictive VI model accuracy by incorporating processes such as biodegradation and multi-species simultaneous vapor transport.

Although VI models have advanced significantly over the past two decades, many of the input parameters used in these models rely on field data collected using traditional point-sampling methodologies. The use of point-sample data for three-dimensional characterization often fails to adequately capture the spatial and temporal scales necessary for optimal predictive VI modeling. Additionally, characterization of site-specific soil properties, such as moisture content, are typically obtained by collecting soil cores and shipping preserved samples to laboratories for analyses. These destructive sampling techniques are incapable of providing continuous measurement of transient soil moisture contents in the unsaturated zone; a dynamic process that has been shown to affect vapor pathway evolution [e.g. *Sakaki et al.*, 2010]. Using sampling methods that remove soil samples from their in-situ environment for analysis has been shown to provide unreliable results for soil characteristics such as moisture content [*Liu*, 2007]. The result of continuing to use these traditional VI site characterization methodologies is an effective bottleneck in the accuracy and reliability of current predictive VI models.

In this work, we address this bottleneck in predictive VI model accuracy by investigating a novel application of electrical resistance tomography (ERT) to characterize key parameters that affect VI pathway evolution on a spatial and temporal scale the far exceeds traditional point-sampling methodologies. Previous laboratory research has shown that the coupling of soil moisture content and soil permeability can have a significant affect on vapor pathway evolution [*Sakaki et al.*, 2010]. The use of geophysical methods such as ERT to capture moisture profiles in the shallow subsurface has been well documented [*Michot et al.*, 2003; *Ozcep et al.*, 2007; *Swartz et al.*, 2008; *Brunet et al.*, 2010; *Franz et al.*, 2011]. Very little research, however, has been conducted using ERT methodologies to characterize vapor-phase related processes. By demonstrating the potential application of ERT as a complementary tool for VI site characterization, the spatial and temporal limitations associated with point-sampling methods can be quickly and cost effectively mitigated.

The results presented in this work demonstrate the potential application of ERT in vapor-phase related site characterization. We have developed a novel VI characterization methodology using ERT by performing intermediate scale, two-dimensional, heterogeneously packed sand tank tests in our laboratory. After evaluating the performance of ERT under controlled laboratory conditions, we tested our ERT characterization methodology in an upscaled environment by performing field demonstrations at a residential VI-impacted site. Our study demonstrates that ERT can potentially be used as a complementary characterization tool at VI-impacted sites. The results presented in this paper will potentially lead to more accurate VI predictive modeling efforts as well as developing a more comprehensive conceptual understanding of the mechanisms that drive the evolution of VI pathways in the unsaturated zone.

CHAPTER 2 – LITERATURE REVIEW

The literature review performed in the following sections provides a through evaluation of previous laboratory and field tests performed using ERT for VI related investigations. At the time of publication, no previous studies have performed VI characterizations using ERT methods. Therefore, the studies evaluated in this literature review were chosen due to investigations into parameters associated with fundamental VI processes. Specifically, this includes parameters such as soil pore moisture content and lithologic composition.

2.1 Vapor Intrusion

The US EPA defines vapor intrusion (VI) as the migration of volatile organic compounds from subsurface sources of contamination to overlying buildings [*USEPA*, 2008]; see Figure 2.1 for conceptual diagram. At representative elementary volume (REV)-scales, two fundamental processes, molecular diffusion and advection, drive vapor intrusion. Molecular diffusion is often the dominant process immediately above the source area as contaminants partition from liquid to vapor phase [*Johnson and Ettinger*, 1991]. At greater distances from the contaminant source zones and at shallower depths, however, advection often becomes the dominant mechanism for vapor transport [*Johnson and Ettinger*, 1991]. These advective mechanisms are driven by pressure differentials which can develop as a result of short-term fluctuations in barometric pressures due to natural oscillations of atmospheric wind and pressure gradients commonly referred to as atmospheric tides, water table fluctuations to due site specific hydrogeology or rainfall events [*Patterson and Davis*, 2009], meteorologically induced long-term changes in barometric pressures [*Keskikuru,* 2001], temperature differentials between the building interior and ambient air [*Garbesi and Sextro*, 1989], wind loading against the side of the building [*Garbesi and Sextro*, 1989; *Keskikuru,* 2001], or centralized HVAC systems [*Garbesi and Sextro*, 1989]. As these pressure differentials develop, vapors in the unsaturated zone can become mobilized, transported laterally, and drawn up into the building's interior space through cracks or gaps in a building's foundation, often lowering indoor air quality below minimum health standards [*Johnson and Ettinger*, 1991; *Hers et al.*, 2000; *Patterson and Davis*, 2009].

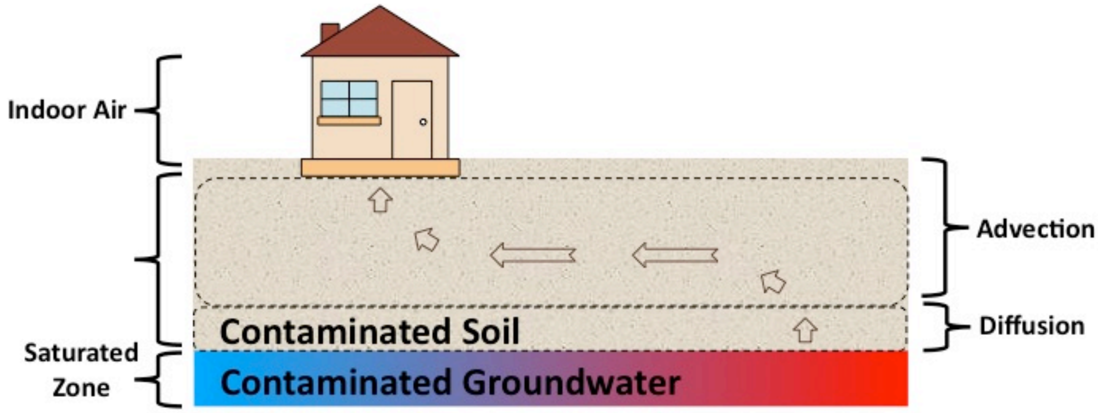

Figure 2.1. General conceptual model of vapor intrusion process driven by diffusion close to the source zone and advection close to the surface.

Over the past two decades, researchers have made significant progress capturing the REV-scale processes that drive vapor intrusion by developing models that can predict vapor-phase mass transport in the unsaturated zone. The earliest VOC-related vapor transport model [e.g. *Johnson and Ettinger*, 1991] adopted many of the conceptual aspects of developed by *Nazaroff et al.* [1988]. *Nazaroff et al.* [1988] pioneered the modeling of radon migration into overlying buildings by performing a series of field investigations that attempted to couple analytical radon concentrations with ambient pressure differences, temperature fluctuations, wind speed fluctuations, and building interior air-exchange rates. Their findings suggested that buildings under pressurization was one of the primarily factors driving the flux of radon decay products into buildings. Building on this pioneering work, many researches have developed mathematical models to predict radon migration into overlying buildings [*Nazaroff*, 1988; *Garbesi and Sextro*, 1989].

Johnson and Ettinger [1991] adopted many of the conceptual processes by *Nazaroff et al.* [1988], developing the first widely used heuristic model for vapor transport into buildings. Their model incorporated both advective and diffusive mechanisms, however, it relied on several major assumptions that greatly oversimplified true field conditions. For example, their model postulated a one-dimensional steady state condition that did not account for subsurface heterogeneities, the formation of preferential vapor pathways, or temporal variations. Their model also assumed an infinite contaminant source (i.e. no mass balance component incorporated into the model) and did not include biodegradation processes.

Since the early nineties, many researchers have built on the work of *Nazaroff et al.* [1988] and *Johnson and Ettinger* [1991] to develop two and three-dimensional predictive vapor intrusion models that incorporate many more of the complex subsurface processes such as transient moisture soil conditions, complex subsurface heterogeneities, and biodegradation that impact the mass transport of vapors into overlying buildings [e.g.; *Mills et al.*, 2007; *Pennell et al.*, 2009].

2.2 Impact of Soil Moisture Content on VI Pathway Evolution

The interaction between soil moisture content and vapor transport in the unsaturated zone is highly coupled. This interaction has been investigated in laboratory and field studies, and through numerical models for many years [e.g. list a few]. For example, *Fitzpatrick and Fitzgerald* [2002] performed a data analysis study that investigated 47 chlorinated solvent contaminated sites in the state of Massachusetts. By using the *Johnson and Ettinger* [1991] model, they were able to compare and correlate observable trends in site conditions at order-of-magnitude scales. Their investigation found soil moisture content to be a highly sensitive parameter in their modeling. This observation was noted in the author's concluding remarks, stating, "infiltrating precipitation can result in the physical displacement and movement of the soil gases."

In an experimental and numerical study performed by *Tillman and Weaver* [2007], the moisture content below and adjacent to VI-impacted buildings was evaluated against observed VI signals inside the buildings. Their study evaluated the use of moisture content values from point samples collected from soil cores adjacent to a building as compared to using moisture content data collected directly beneath the VI-impacted building. *Tillman and Weaver* [2007] used a variably saturated water flow model (HYDRUS-2D) to process data from two years of local hourly rainfall measurements in a simulated VI-impacted building slab. The moisture content values where then incorporated into the *Johnson and Ettinger* [1991] risk assessment model. *Tillman and Weaver* [2007] concluded, conceptually, that the diffusion of vapors through the unsaturated zone occurs along channels of air-filled pore spaces within the soil matrix, and that the spatial and temporal variability of soil moisture contents may constrain the mass transport of vapors and consequently the vapor intrusion risk [*Tillman and Weaver*, 2007]. This study highlights the highly coupled relationship between soil moisture content and vapor mass transport in the unsaturated zone.

In a recent laboratory study, *Sakaki et al.* [2011] performed a series of intermediate scale two-dimensional sand tank tests and evaluated the impact of surface moisture events (i.e. rain events) on VI pathway evolution. Their results indicate that redistributions of soil moisture contents can significantly alter the mass transport of vapor-phase compounds in the unsaturated zone. The conceptual model postulated by their research suggests that natural surface events such as precipitation create wetting fronts that infiltrate and migrate down into the unsaturated zone, as seen in Figure 3. As this wetting front migrates down, the water preferentially fills the pore space of the porous media with the lowest pore entry pressure. As water infiltrates and fills the pore space, vapors are displaced. The displacement of vapors in the soil pores creates a compression effect that potentially drives vapors into overlying buildings. Observational results from *Sakaki et al.*, [2011] demonstrate that this compression effect can result in spikes in the VI signal as the vapors are physically displaced by the infiltrating wetting front. If the wetting front contains enough water volume, the pore space can become completely saturated, causing the transmission of vapors to cease through that localized pathway.

Recent laboratory experiments performed by researchers such as *Sakaki et al.* [2011] have successfully demonstrated the significant impact of surface moisture events on VI fluxes through physical VI models. These findings are consistent with previous observations made in other VI related field studies [e.g. *Fitzpatrick and Fitzgerald*, 2002]. The research conducted for this study investigates this complex and highly coupled relationship between soil moisture content and VI pathway evolution dynamics in the unsaturated zone.

2.3 ERT Theory and Applications

The use of geoelectrical techniques, such as ERT, to define subsurface structures dates back to the early twentieth century when Conrad Schlumberger conducted the first geoelectrical resistivity surveys in the fields of Normandy in 1912 [*Kunetz*, 1966]. Over the last century, geoelectrical resistivity survey techniques have improved significantly. As a result of these advances, geoelectrical resistivity techniques have become a critical instrument used in hydrogeological studies, mining exploration, engineering projects, and environmental investigations [*Griffiths et al.*, 1990; *Griffiths and Barker*, 1993; *Dahlin and Loke*, 1997; *Olayinka*, 1999; *Olayinka and Yaramanci*, 1999; *Amidu and Olayinka*, 2006; *Aizebeohai et al.*, 2009, 2010].

ERT methods are based on the general theory that electric fields, caused by a introducing a current into the ground, can be observed and interpreted to represent material properties of subsurface compositions [*Sheriff*, 2004], see Appendix A.1 for additional information. By rearranging the electrode positions used in ERT surveys, several different types of electrode arrays can be constructed, each with distinct advantages and disadvantages, see Appendix A.2 for additional information. For field applications, the array chosen depends on several factors such as, the site subsurface heterogeneity, the types of structures being delineated, background noise levels, sensitivity to vertical or lateral delineations, depth of investigation required, spatial data coverage required, and signal strength of the array [*Dahlin and Loke*, 1997]. See Appendix A for additional ERT background information.

2.4 Previous Work Evaluating ERT in Laboratory Experiments

In the past decade and a half several studies have performed ERT evaluations in laboratory experiments that have investigated subsurface processes that are indirectly related to vapor intrusion. To date, there have been no laboratory studies, that the author of this paper is aware of, that have used ERT methodologies to directly address a vapor intrusion related problems. However, several studies have used ERT to capture key vapor intrusion related parameters such as soil moisture content [*Daily et al.*, 1995; *Slater et al.*, 2002; *Franz et al.*, 2010]. The following sections will severe as a review previous laboratory experimentation that used ERT to investigate REV-scale processes that impact vapor intrusion.

In one of the earlier examples of ERT-related laboratory experiments, *Daily et al.* [1995] were able to demonstrate the utility of ERT in environmental applications such as delineating leaked contaminant distributions in the subsurface, monitoring aspects of remediation such as air bubble radius of influence during air sparging, and detecting leaks from underground storage tanks. All three tests were performed in an intermediate scale sand filled testing tank. The air sparge tests were performed in saturated soil conditions. The air bubbles were released from the bottom of a single vertical pipe inserted in the center of the test tank. ERT profiles were performed along the surface and from two bore holes located inside the test tank before, during, and after the air sparging event. They found that ERT was unsuccessful at distinguishing individual air bubble channels but was able to distinguish a bulk perturbation. In their contaminant release tests, they released a metered amount of gasoline on the soil surface. They performed ERT profiles, before, during and after the spill event. The results of this experiment demonstrated that ERT was able to delineate the area of impact under saturated and unsaturated conditions. Their third experiment attempted to capture a spill from an underground storage tank by releasing a metered amount of water for a buried steel vessel. The results for this experiment showed the ERT was unable to capture the leaking water directly below the steel vessel but that it was successful at capturing the leaked water at a minimum distance from the bottom of the steel vessel.

In a later study performed by *Slater et al.* [2002] ERT was used to capture solute transport processes. Their study used an intermediate scale sand tank apparatus to evaluate ERT performance through surface and borehole surveys. The experimentation performed in this study was designed to expand on the previous ERT investigations involving solute transport processes performed by *Slater et al.* [2000]. In this study, the researchers used time series ERT measurements to attempt to revolve voxel breakthrough curves in an attempt to capture the controlled release of a tracer (NaCl). They then compared the breakthrough curves with direct measurements of fluid conductivities measured in the sand tank and against predictions using a three –dimensional finite-element coupled flow and transport model. Their results indicated a general agreement of ERT voxel response to direct fluid conductivity measurements, however, discrepancies did occur at early time-series measurements. In their discussion section, they attributed the early time discrepancies to differences in image voxel scales versus the fluid conductivity measurements, which resulted in ERT measurement errors being transmitted into inversion schemes. Additionally, when comparing the ERT inversion with predicted flow and transport models, the researchers found good agreement.

In a more recent study, *Franz et al.* [2010] attempted to quantify soil moisture contents using ERT techniques in an intermediate scale three dimensional sand tank apparatus. The researchers in this study used ERT to capture spatial and temporal changes in soil moisture contents due to a rapid infiltration event. For this experiment, the researchers wet-packed homogeneous sand (ASTM #20/30), in an effort to reduce the build up of fine particles between packed layers. After wet-packing the sand tank, the researchers applied a metered volume of water to the surface of the soil in an effort to create an infiltration event and then allowed the system to drain for two days. ERT surveys were collected from 12 borehole electrode stacks before, during, and after the infiltration event. Rather that perform inversions on the resistivity measurements, as has typically been done in the past, this study approached the quantification of soil moisture contents by directly converting their resistivity measurements to soil moisture contents using Archie's relationship. The ERT observations were then compared to a two-dimensional, axi-symmetric, numerical solutions using HYDRUS 2D/3D software and to a semi analytical solution using direct measurements taken from soil cores. This study found acceptable levels of agreement between the observed data and numerical and semi analytical predictions.

2.5 Previous Work Evaluating ERT in Field Studies

Several studies over the past decade have performed ERT evaluations in field studies, investigating subsurface processes indirectly related to vapor intrusion. To the author's best knowledge, there have been no field studies to date that have used ERT methodologies to directly address vapor intrusion related problems. However, several studies have used ERT to capture key vapor intrusion related parameters such as soil moisture content and soil horizons, but not VI directly [*Michot et al.*, 2003; *Ozcep et al.*, 2009; *Swartz et al.*, 2008; *Brunet et al.*, 2010; *Franz et al.*, 2010]. The following section reviews field studies that used ERT to investigate REV-scale processes such as soil moisture content and soil horizons.

Michot et al. [2003] investigated the ability of ERT to capture the change in shallow soil water content of an irrigated corn crop. They were able to use ERT methods to characterize soil drainage through water uptake by roots, the progression of the infiltration front with preferential flow zones, and the drainage of the plowed horizon. More recently, *Schwartz et al.* [2008] successfully combined ERT methods combined with time domain reflectometry (TDR) to simultaneously measure soil resistivity and soil moisture at a field site. The objective of this study was to attempt to quantify soil moisture along two-dimensional unsaturated zone profiles. The authors used bulk conductivity derived from ERI models of soil resistivity, pore water conductivity derived using an exchangeable cation proxy (Ca + Mg), and percent clay content of soil, to convert two-dimensional ERI profiles into two-dimensional soil moisture profiles.

A more recent study by *Brunet et al.* [2010] demonstrated the application of ERT to quantify soil moisture content and soil water deficit (the difference between effective porosity and water content) at a field site in southern France. They found ERT to be advantageous for their study due to its nonintrusiveness, its ability to exhibit spatial patterns at large scales, and the quality of information produced for both water content and soil depth values.

The aforementioned field studies illustrate the documented performance of ERT to quickly and effectively capture the dynamic changes in soil moisture contents that the unsaturated zone undergoes, as well as soil horizons at the spatial and temporal scales that are required for effective vapor intrusion modeling. The research presented in this paper builds on the previous work performed using ERT in hydrogeological applications by addressing the need to develop novel approaches to improve VI characterization techniques.

CHAPTER 3 – RESEARCH QUESTIONS OUTLINING ERT EXPERIMENTATION AND EVALUATION

The overall goal of this experiment was to investigate geophysical methods that could improve spatial and temporal characterization of VI pathways. We approached this objective by determining which subsurface parameters affect VI pathway evolution and developing a set of research questions that effectively incorporate these parameters while testing ERT for VI pathway characterization. These parameters were evaluated through literature reviews and previous intermediate scale sand tank experiments conducted at the CESEP laboratory [*Sakaki*, 2011]. Our experiments, as well as other previous studies [e.g. *Fitzpatrick et al.*, 2002], have demonstrated that relative soil moisture contents and relative lithologic permeabilities are two of the most sensitive parameters affecting vapor transport dynamics in the subsurface. Results from previous studies such as these indicate that mass transport through VI pathways is significantly affected by redistributions of soil pore moisture contents and spatial differences in soil permeabilities. These findings suggest that climatic surface moisture events, such as precipitation, create wetting fronts that move downward through the unsaturated zone, altering vapor flow paths by compressing and displacing vapor flow paths.

Figure 3.1 shows a conceptual model that illustrates the surface distribution of moisture and the compression effect on VI pathways that can result from the wetting front migrating downward. By combing the information obtained experiments and literature reviews, we developed the following set of research questions to evaluate ERT for VI characterization applications:

Research Question #1: Can ERT be used as an effective tool to characterize relative soil moisture distributions and lithologic compositions in heterogeneous soil formations, thus identifying potential preferential VI pathways?

To address this question, we focused on developing a physical VI model that would allow us to test and evaluate ERT under controlled boundary conditions. Our physical model was based on REV-scale VI processes that incorporated the effect of

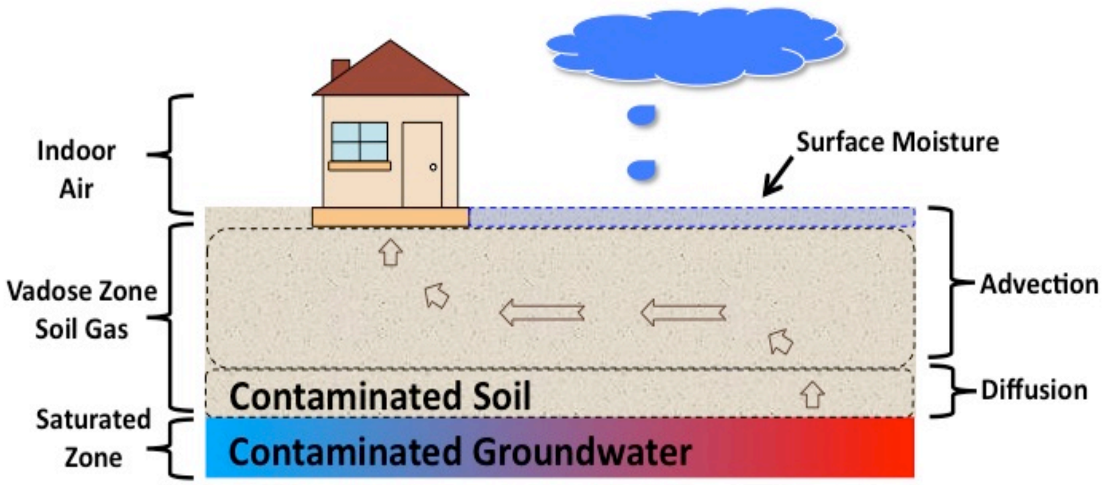

Figure 3.1. Conceptual model of surface moisture event infiltrating the vadose zone and compressing the zone for vapor transport.

moisture redistributions and lithologic contrasts in the unsaturated zone. Figure 3.2 shows a REV-scale conceptual model of these hydrogeologic processes that drive VI.

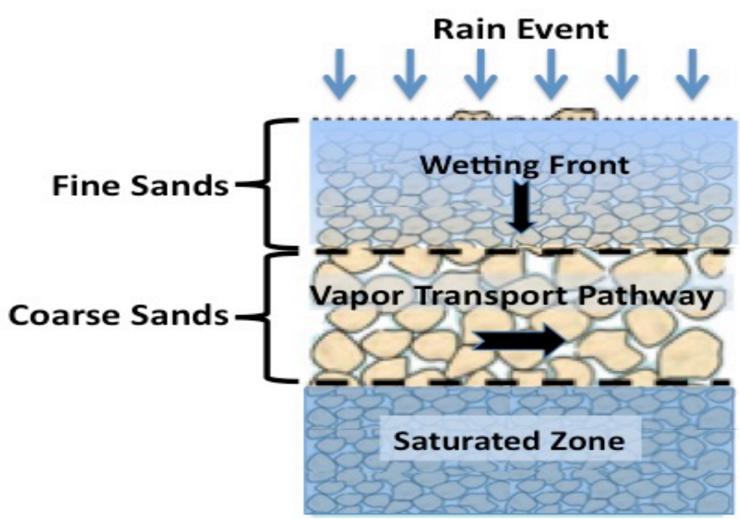

Figure 3.2. Representative elementary volume (REV)-scale hydrologic processes that contribute to the evolution of vapor transport pathways.

Several pervious studies have evaluated ERT in controlled laboratory settings [*Daily et al.*, 1995; *Slater et al.*, 2002] and have shown encouraging results capturing parameters associated with VI processes. These previous studies, demonstrate that ERT is capable of capturing dynamic moisture redistributions in the shallow subsurface. *Daily et* *al.*, [1995] used an intermediate-scale sand tank apparatus to test ERT. They performed ERT experimentation to capture subsurface processes associated with in-situ remediation processes such as characterizing a gasoline spill and imaging the radial influence of bubble formation associated with air sparging, finding that ERT was capable of distinguishing the regions infiltrated with air bubbles. *Slater et al.*, [2002] also performed several intermediate scale sand tank experiments. They were able to successfully demonstrate ERT as an effective tool to monitor solute transport in large tank experiments. They used high resolution cross borehole 3D ERT surveys in time series sequences to evaluate solute transport data imaging against modeled break through curves and well data. Testing of ERT methodologies for VI characterization applications, however, also requires testing lithologic compositions that simulate VI environments. VI processes depend not only on relative moisture contents in the zone of vapor transport, but also on relative permeabilities. The most permeable lithologic layers provide the framework for channel formation that allows VI processes to develop. On a REV-scale these vapor channels are the interconnected soil pores in the most permeable lithologic layers. Our first research question was developed to test the performance of ERT in capturing these REV-scale interconnected soil pore pathways under various moisture content conditions.

Our second research question was designed to test the ERT VI pathway characterization methodologies developed in the laboratory, in an upscaled environment, through a series of field demonstrations at a site with active VI processes. This research question also focuses on evaluating ERT performance at REV-scales. By developing research questions that focus on fundamental principals operating at REV-scales, our ERT evaluations will provide novel fundamental qualitative information about the mechanisms that drive VI in the unsaturated zone.

Research Question #2: Can VI characterization methodologies developed in a laboratory setting using ERT be successfully applied to an active VI site to provide valuable qualitative information about VI pathway evolution through a novel joint-interpretation of soft geophysical data with hard analytic data?

Several field studies have shown that ERT can effectively characterize parameters associated with VI pathway evolution dynamics. For example, *Michot et al.*, [2003] were able to use ERT to capture soil water flow dynamics in cornfields, including soil drainage though water uptake by roots and progression of the infiltration front during irrigation. *Schwartz et al.*, [2008] used ERT in a field study to quantitatively determine soil moisture contents in the shallow subsurface. This study used time-series ERT data sets and applied a modified version of *Archie's Relationship* to develop quantitative 2D soil moisture profiles. Although studies like these have successfully demonstrated that ERT can capture shallow subsurface flow dynamics and moisture contents, effective VI pathways characterization must also capture relative lithologic permeabilities. Subsurface vapor flow mechanics follow basic laws of gas diffusion and migrate from zones of high pressure to zones low pressure along the channels of least resistance. At field-scales, these vapor channels are formed by interconnected pore spaces in the lithologic layers with the highest relative permeabilities. Our second hypothesis predicts that ERT is capable of capturing relative moisture contents and lithologic contrasts used to determine vapor pathway evolution.

CHAPTER 4 – OBJECTIVES AND TASKS

The primary objective of this work was to investigate the novel application of ERT as a VI characterization tool to identify preferential vapor flow paths in the unsaturated zone by capturing lithologic and soil moisture contrasts. To accomplish this objective, we designed a series of laboratory experiments based on the REV-scale processes outlined in Figure 3.2. The laboratory experiments incorporated the REV-scale processes in a physical VI model built in the CESEP laboratory. After performing our laboratory ERT evaluations we then performed a qualitative field demonstration to test the research questions outlined in the previous sections. The field demonstrations served as a proof-of-principle demonstration to evaluate the practical applicability of ERT under highly complex field conditions.

4.1 Task 1 – Intermediate Scale Laboratory Sand Tank Experiments

This task was designed to evaluate the performance of ERT in characterizing soil moisture distributions and lithologic compositions in saturated and unsaturated environments under controlled laboratory conditions. This was accomplished by conducting a series of laboratory experiments using an intermediate-scale, sand tank apparatus. The sand tank experiments allowed us to develop an understanding of the fundamental REV-scale hydrologic processes, such as variable pore-moisture content under drainage cycles, that effect ERT performance in a simplified and controlled environment. The primary objective of our sand tank experiments was to test the performance of ERT in capturing heterogeneous-packed configurations under various water content conditions. We selected three heterogeneous packing configurations that represented simplified VI lithologic settings to evaluate the impact of pore-moisture content during ERT performance evaluations. Each of the selected packing configurations served as simplified VI physical models. Each configuration captured geologic field conditions such as horizontal deposition of interbedded coarse layering commonly associated with VI conditions allow for lateral transport of contaminant vapors in the unsaturated zone. The first packing configuration was designed as to represent the simplest lithologic composition, with each additional packing configuration becoming more complex. Using several packing configurations with varying degrees of complexity allowed for ERT evaluation over a wider range of potential field conditions. By controlling the water table, we were able to test all three sand-pack configurations at various saturations.

4.2 Task 2 – Proof-of-Principle Field Demonstration

After performing a through evaluation of ERT capabilities at intermediate-scales, we up-scaled the experimentation to test the methodology developed in the laboratory at field-scale conditions at a site with an active VI signal present. One of the primary principals guiding the research conducted in the laboratory is the concept of practical up-scalability. This concept focuses on evaluating fundamental pore-scale processes at bench or intermediate scale in a controlled laboratory setting and testing the knowledge or methodology in a more complex up-scaled field environment. Task 2 was designed to test the geophysical methodology developed in our laboratory at a field-scale environment with active VI signals. The field demonstration was conducted at a Department of Defense (DoD) site with a known dissolved-phase chlorinated solvent plume creating observable VI signals at sub-slab, interior and exterior soil gas sampling points. The goal of Task 2 was to collect soft ERT data that could be processed and compared to hard point-sample VI data. The approach to our field demonstrations included creating an induced and controlled moisture event at the surface, with the expectation that the impact of this surface event would be observable in both the soft geophysical data and the hard VI data.

4.3 Field Demonstration - Site Background

The site selected for field demonstrations is currently owned and operated as a SERDP-funded field study site by Professor Paul Johnson from Arizona State University (ASU). The field site is located in Layton, Utah, as seen in Figure 4.1.

Figure 4.1. Map with field demonstration site location (indicated by red star) located at Hill AFB.

The site selected for this field demonstration is a residential home that has been converted to a field study site by Professor Johnson's research group from ASU. The site is adjacent to Hill Air Force Base (AFB) and is one of many homes in the area that the DoD has identified as a site with compromised indoor air quality due to VI related mechanism. Groundwater contamination on the site consists of a dissolved-phase chlorinated solvent plume containing trichloroethylene (TCE) as the primary chemical of concern (COC). This contaminated groundwater plume, along with the associated contaminated pore-water in the capillary zone produces observable VI signals on-site. Soil gas measurement points include interior sub-slab, above slab, interior ambient, and exterior subsurface locations (at three-foot depth increments from surface to groundwater elevation located at approximately 15 ft bgs). Professor Johnson's research group has installed a sensor and sampling network that covers the entire building envelope (interior and sub-slab) and six exterior subsurface regions around the building, as seen in Figure 4.2.

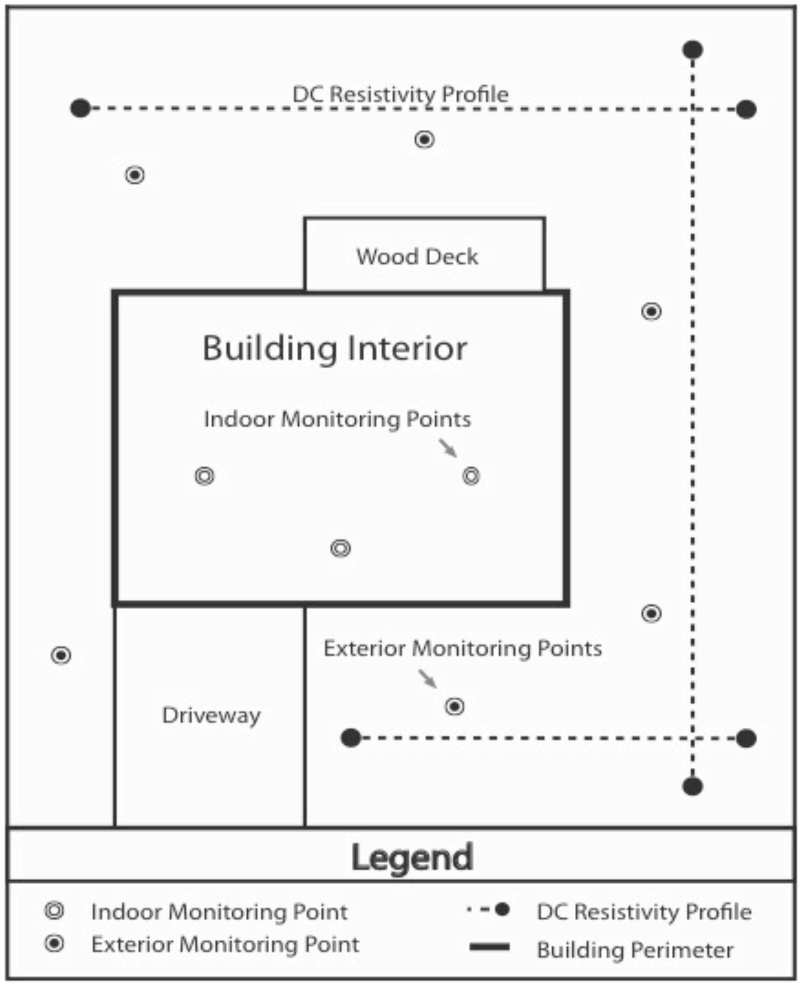

Figure 4.2. Schematic of VI monitoring locations with exterior and interior monitoring points indicated by concentric circles (oxygen concentrations, pressure potential, and soil gas sampling ports) and ERT profiles indicated by dashed lines with solid circular ends.

The sensor and sampling networks consist of O_2 sensors, pressure transducers, and soil-gas monitoring points in the unsaturated zone surrounding and below the building envelope. Their soil-gas monitoring program is autonomous and continuous. It utilizes an on-site soil-gas collection system, which automatically collects and runs samples thorough an on-site gas chromatograph/mass spectrometer (Hapsite GC/MS, Inficon, Syracuse, New York) every four hours. The group has installed a MET station in the back yard to record key atmospheric data sets such as precipitation, rain, humidity, temperature, and wind speed. They have installed a depressurization system in the second floor, allowing them to create artificially high, pressure gradients in the subsurface. The depressurization system is designed using commercially available 24-inch box fans, sealed in the upper bedroom windows, used to push interior air outside the building, effectively lowing the interior pressure relative to exterior atmospheric pressure. These pressure gradients drive the advective transport of COCs. By creating a mechanism (the box-fan depressurization system) to manipulate these pressure gradients, the ASU group was able to study VI processes in a more dynamic environment. Professor Johnson's field study was designed as a two-stage study - Stage 1 was a baseline evaluation performed under normal living conditions, and Stage 2 was an induced high-pressure condition. The induced high-pressure condition was designed to take advantage of advective processes that transport vapors and create a higher than normal VI signal.

4.4 ERT Field Demonstration – Technical Approach

Initial evaluations of site geology indicated highly heterogeneous conditions composed primarily of silts/clays with interbedded fine sand stringers that span from approximately 3 ft below ground surface (bgs), to the water table, located approximately 15 ft bgs, as seen on Figure 4.3 (a) and (b). Based on this initial geologic interpretation and previous VI laboratory research [*Sakaki et al.*, 2011], we determined to most likely avenues of vapor transport to be the interconnected fine sand stringers due to their lower relative pore entry pressures and drainage characteristics. The fine sand stringers ranged from less than 1 inch to approximately 4 inches in thickness and the water table ranged from approximately 14 ft bgs to 16 ft bgs. Based on this initial evaluation of site geology and the water table depth, the total depth of penetration (DOP) for our ERT field demonstration was determined to be approximately 15 ft. Using a 28 electrode Wenner surface profile, this DOP required an electrode spacing of approximately 3.5 ft. The thickness of the fine sand stingers observed in the field would later be used to determine the final thickness for packed heterogeneities in our laboratory sand tank tests.

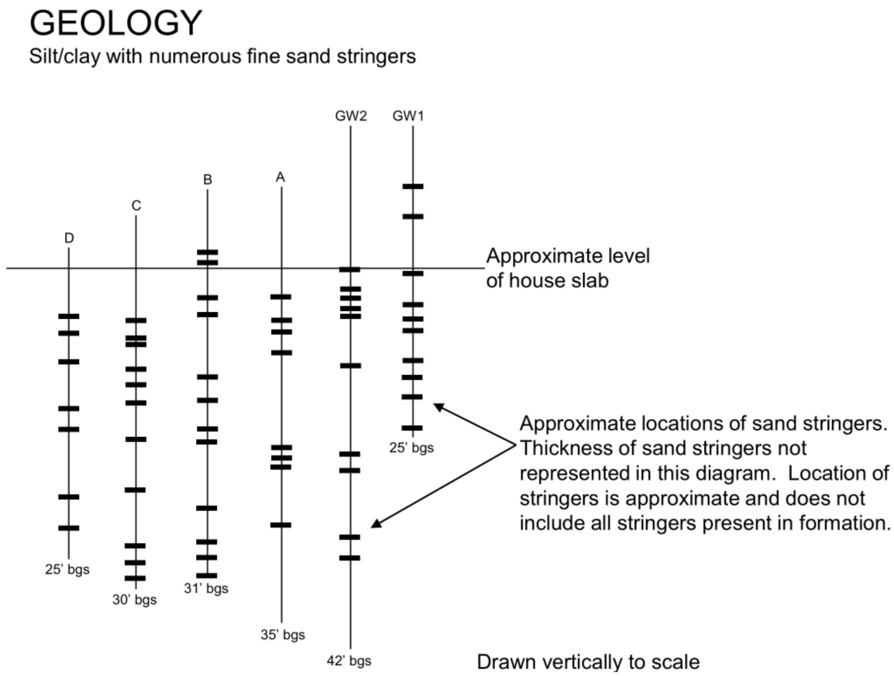

Figure 4.3 (a). Schematic of subsurface geologic composition at field demonstration site in Utah [*Ongoing VI site study by Johnson et al.*, 2010-2012].

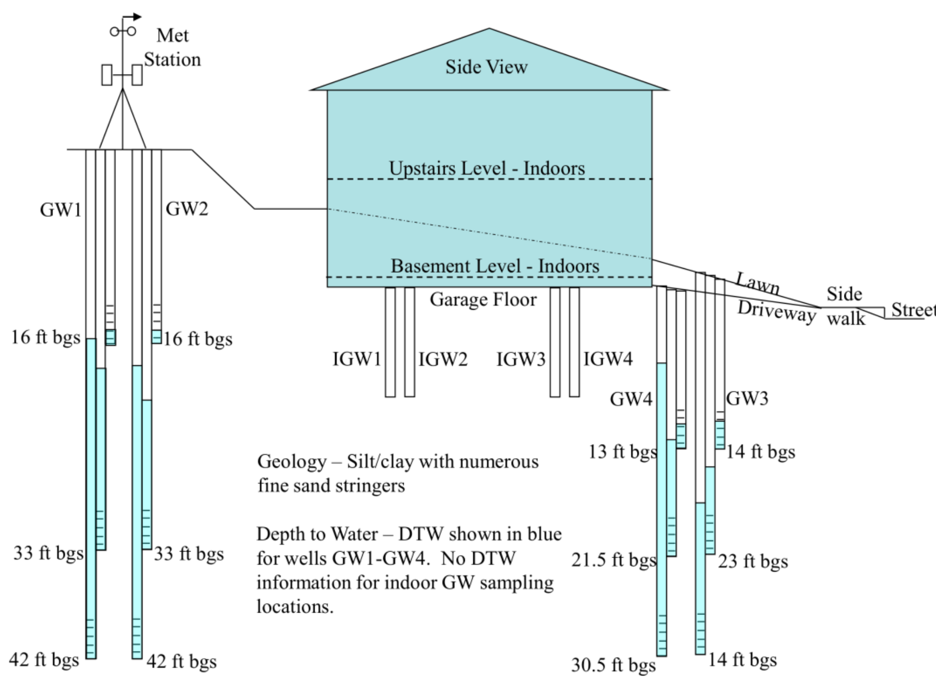

Figure 4.3 (b). Schematic of water table elevations across field demonstration site [*Ongoing VI site study by Johnson et al.*, 2010-2012].

Initial evaluations of pressure differential data and VI concentrations collected by Professor Johnson's field research team suggested a correlation of maximum/minimum VI signals with maximum/minimum applied pressure differential signals [*Ongoing VI site study by Johnson et al.,* 2010-2012]. This condition is created as a result of pressure differentials between the building's interior and exterior/ambient pressures. Based on our evaluation of this pressure differential – VI data relationship, our conceptual model suggested that during the summer months, normal use of a central AC unit created a high-pressure zone inside the building, leading to lower VI signals. During colder winter months, however, the normal use of a central heating unit created a low-pressure zone inside the building, creating high pressure differentials (relative to exterior pressures) and corresponding peak VI signals. These strong pressure differentials drive advective transport through the soil vapor pathways, which lead to peak VI during the winter months. In an effort to develop a relationship between VI signals and redistributions of subsurface moisture content captured by soft geophysical techniques, our research group determined it was critical that all ERT field demonstrations correspond with periods of strong observable VI signals.

The technical approach for our field demonstration was to design an experiment that could evaluate the degree ERT performance in characterizing relative moisture distributions and lithologic compositions in the unsaturated zone under VI conditions. To establish a baseline profile for moisture and lithologic conditions in the subsurface, we performed an initial ERT survey with no disturbances to the system. This initial survey was followed by an induced moisture event at the surface (created using the in-place sprinkler system). We were able test our hypothesis about the effect surface events have on vapor pathway evolution by creating this induced moisture event and comparing the before and after ERT data to the before and after VI data. By creating an event that was observable in both our ERT data and our analytic data we were able to establish a novel coupling of soft and hard data sets associated with VI mechanisms.

CHAPTER 5 – MATERIALS AND METHODS

The material and methods used for all laboratory experimentation and field demonstration were selected based on the ability to produce repeatable tests (See Appendix C for additional information about equipment used for this study). The laboratory sands selected were laboratory grade, well-characterized sands. All sensors used were designed for continuous use in wet or dry environments. The ERT unit was selected due to it robust design and multi-electrode multi-channel design. All laboratory experiments were performed at the Colorado School of Mines (CMS) Center for Experimental Study of Subsurface Environmental Processes (CESEP) laboratory under a SERDP-funded grant (See Appendix B for additional SERDP project background information).

5.1 Design of Experimental Apparatus

To test our hypotheses about the effects of moisture content redistributions on VI pathway evolution dynamics and the potential application of ERT for VI site characterization, we performed a series of controlled laboratory experiments. All laboratory experimentation was conducted in an intermediate-scale two-dimensional sand tank apparatus constructed using 5/8”-thick clear plexiglass panels for front, rear, bottom, and sides (length = 220 cm, width = 8.25 cm, height = 110 cm). The panels were sealed using clear silicone and bolted together using stainless-steel hardware. The top of the sand tank was left open to the atmosphere to allow access for geophysical instrumentation. The sides of the sand tank contained water drainage points connected to vertically adjustable external reservoirs (diameter = 8 cm, height = 15 cm), as seen in Figure 5.1. An array of soil moisture sensors (ECH$_2$O EC-5, prong length = 5.5 cm, measurement frequency = 70 MHz, Decagon Devices Inc., Pullman, WA) were installed at vertical depths (4, 14, 25, 30, 35, 40, and 55 cm bgs) required to capture the sand-pack heterogeneities, changes in soil moisture contents, and changes to adjusted water table elevation throughout the experimentation. All sensors used on this experiment were

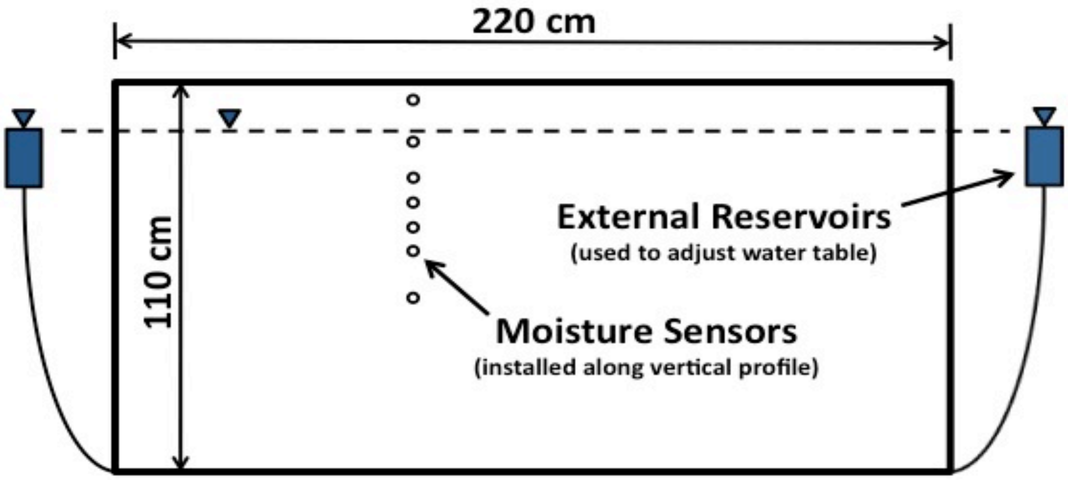

Figure 5.1. Schematic of the sand tank apparatus dimensions with reservoirs used to control water table elevation and moisture sensors installed along a vertical profile (not drawn to scale). Moisture sensors are installed at depths of 4, 14, 25, 30, 35, 40, and 55 cm bgs (below ground surface). Total volume of sand tank is 163,350 cm^3.

installed through the vertical walls of the test tank to avoid water channeling on the sensor wires and to keep the surface clear for geophysics equipment. Two temperature probes (EC-T, Decagon Devices Inc., Pullman, WA) were installed through the walls of the sand tank apparatus at depths of 5 cm bgs and 80 cm bgs in order to capture any temperature variations throughout experimentation. All sensor output signals were recorded by self-contained, digital data loggers (EM50, Decagon Devices Inc., Pullman, WA) designed to power, read, and log data from compatible sensors. See Appendix C-2 and Appendix C-3 for additional information about sensors used in this study.

The first step in processing the moisture sensor data (ECH$_2$O EC-5, Decagon Devices, Pullman, WA) is performing a calibration of the raw sensor data collected during experimentation. To perform this calibration, the raw signal produced by the ECH$_2$O EC-5 moisture sensor (mV range) is transmitted to a compatible data logger (Em50 data logger or ECH$_2$O EC-5 check hand-held reader, 12-bit, excitation voltage = 3V, Decagon Devices, Inc., Pullman, WA) and automatically converted into an analog-to-digital converter number (ADC). The ADC number is then converted to soil moisture content values by incorporating the non-linear two point α-mixing model developed by *Sakaki et al.* [2008]. Applying the two point α-mixing model [*Sakaki et al.*, 2008] for sensor data calibration requires obtaining two matrix specific measurements; one measurement of the ADC reading in totally dry sands and one measurement of the ADC reading in completely saturated sands. Once these two values are collected, the non-linear relationship shown in Equation 5.1 can be applied.

$$\theta = \frac{ADC^{\alpha} - ADC_{dry}^{\alpha}}{ADC_{sat}^{\alpha} - ADC_{dry}^{\alpha}} \Phi \tag{5.1}$$

where ADC_{sat} is the ADC count value for a water-solid mixture in saturated conditions, ADC_{dry} is the ADC count for the air-solid mixture in dry conditions, θ is the volumetric water moisture content, and Φ is the porosity of the porous medium. After performing the two-point α-mixing model calibration to all observed soil moisture data, I was able to calculate the volumetric moisture contents and effective saturations for the packed sands.

5.2 Geophysical Instrumentation

A SuperSting R8 IP 8-channel earth resistivity meter (Advanced Geosciences Inc., Austin, TX) with 28 stainless steel electrodes was used to perform the ERT surveys along surface profiles in the sand tank. An electrode spacing of 6.25 cm, shown in Figure 5.2 (a), was selected based on the spatial resolution and depth of investigation required to capture the sand-pack heterogeneities. For ERT investigations, as the electrode spacing decreases, the depth of investigation decreases proportionally and the resolution increases [*Sheriff*, 2004]. Our experiments required an approximate depth of investigation of 45 cm (to capture the packed heterogeneities) and a spatial resolution fine enough to capture a 4 cm.-thick horizontal layer (used in sand-pack configuration #3).

To assess which geophysical electrode array configuration would result in the most accurate representation of the heterogeneous-packed configurations selected for this experiment, several feasibility tests were performed in the spring of 2011. The two arrays used in the feasibility tests were Wenner and Dipole-Dipole. Although the inversion of data obtained from each of the array configurations provided positive results (i.e. the reconstructions created by the inversion process clearly identify the known sand tank compositions), the Wenner configuration recovered the original model slightly better and with less data required. Based on these numerical simulations, the Wenner electrode array was selected as the best configuration for the conditions we were testing. The electrodes were made of round-stock stainless steel, measured approximately 8 cm. (length) by 1 cm. (diameter), and were inserted directly into the sand surface Figure 5.2 (b). The SuperSting main data cable was connected to the electrodes using plastic coated 18-gauge aluminum wire and secured using 2 in. aluminum alligator clips Figure 5.2 (c). Figures 5.2 (a-c) show the SuperSting R8 IP 8-channel earth resistivity meter components, (a) is a photo of the electrode spacing used, (b) is a close-up photo of the electrodes being inserted directly into the soil surface, (c) is a photo showing electrical components used to connect electrode circuits to main ERT data cables. See Appendix C-1 for additional information.

Figure 5.2 (a-c). (a) Photo of the electrode spacing (approximately 6.25 cm) along a surface profile (b) Close-up photo of the electrodes being inserted directly into the soil surface (c) Photo showing electrical components used to connect electrodes to main ERT data cables.

5.3 Sand Material

Three uniform specialty silica sands, Accusand (Unimin Corp., Ottawa, MN) #12/20, #20/30, and Granusil #70 (identified by the effective sieve number and sold as Accusand 12/20, 20/30, and Granusil 7030, respectively) were used. The manufacturer's technical sheet for Accusand #12/20 and #20/30 reports a uniformity coefficient of approximately 1.2, grain size density of 2.66 g/cm^3, grain shape classification of rounded, and composition of 99.8% quartz. For Accusand #70, the technical sheet specifies a uniformity coefficient of approximately 1.7, grain size density of 2.65 g/cm^3, and grain shape classification of sub-angular. Selected important properties of the specialty sands are summarized in Table 5.1. The soil water retention curves for all three sands used in the experiment can be seen in Figure 5.3. The curves were calculated using van Genuchten parameters, estimated using the established soil properties from *Smits et al.* [2010].

Table 5.1. Select properties of specialty silica sands used in laboratory experimentation.

Sand No. - Manufacturer	Sand Properties[1,2] (tightly-packed)			van Genuchten Parameters[3]	
	Porosity [-]	h_d [cm of water]	d_{50} [mm]	α [cm^{-1}]	n (m=1-1/n)
#12/30 - Accusands	0.312	7.0	1.040	0.0100	9.21
#20/30 - Accusands	0.330	12.0	0.750	0.0528	9.32
#70 - Granusils	0.413	41.2	0.200	0.0210	11.53

[1] 2009 characterization of #12/20 and #20/30 sands (Smits and Limsuwat)

[2] 2007 characteization of #70 sand (Limsuwat and Sakaki)

[3] van Genuchten parameters obtained using RETC

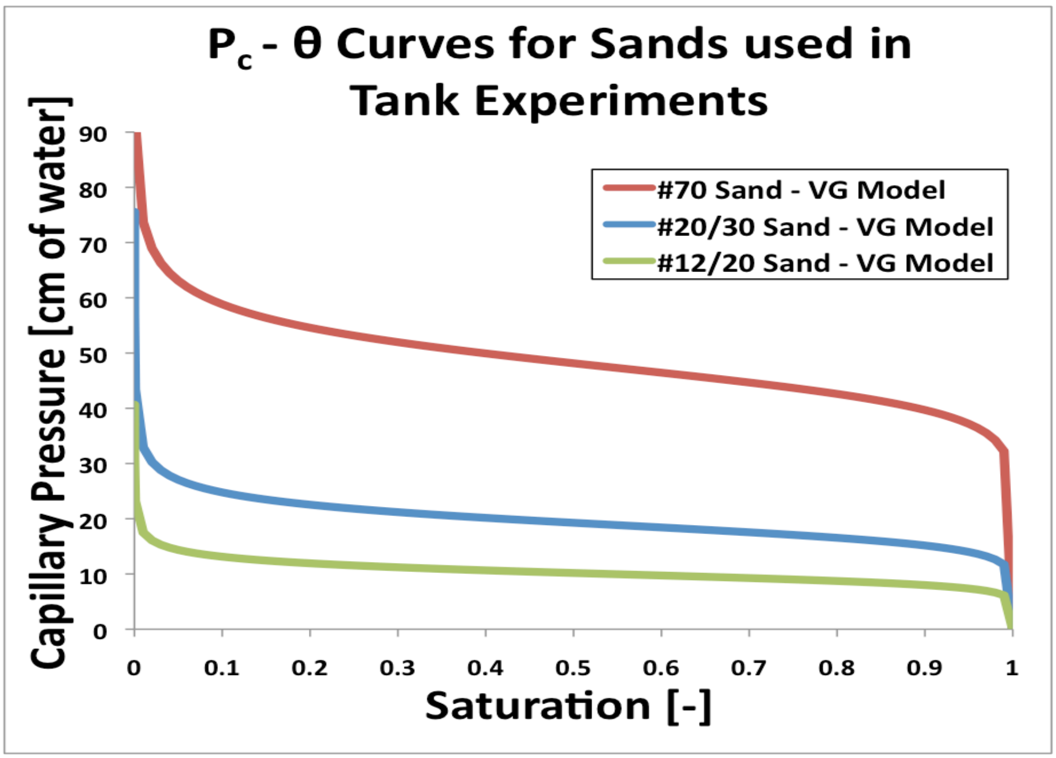

Figure 5.3. Soil water retention functions [*van Genuchten,* 1980] for all three sands used in laboratory sand tank tests (#70, #20/30 and #12/20).

5.4 Experimental Procedure

The tank was carefully wet-packed using well-characterized crushed silica sands in three unique, simplified heterogeneously-packed configurations, as seen in Figure 5.4. During the wet-packing procedure, the sand was carefully poured into the tank using a sieve in incremental layers of approximately 2 cm. The depth of the water in the tank was kept constant at approx. 12 cm in order to minimize layering in the tank. We were able to achieve maximum packing density by physically disturbing the wet-packed surface after each sand layer was deposited, and by tapping the walls of the sand tank during and after each sand layer was deposited; this method has been documented to achieve higher packing density than the methods outlined by ASTM D 4253-00. The use of a vibratory device has also been documented to help achieve higher packing densities (ASTM D 4253, 2006), however, due to our dense network of sensitive sensors, we elected to refrain from using a vibratory device.

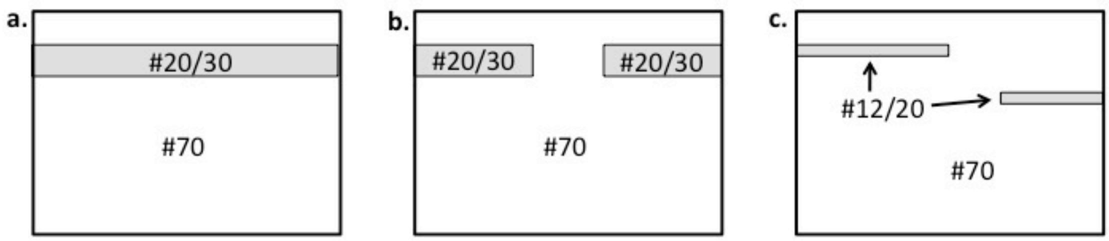

Figure 5.4 (a-c). (a) Schematic of sand tank packing *Configuration #1* – Fine matrix (#70 sand) with coarse horizontal layer (#20/30 sand, 10 cm. thick). (b) Schematic of *Configuration #2* – Fine matrix (#70 sand) with coarse discontinuous horizontal layer (#20/30 sand, 10 cm. thick). (c) Schematic of *Configuration #3* - Fine matrix (#70 sand) with shallow and deep thin discontinuous horizontal layers (#12/20, 4 cm. thick). Figures not drawn to scale.

For each packing configuration, the water table was initially established at the top of the sand tank. ERT profiles were taken under saturated conditions for each packing configuration. The bottom and side boundaries of the tank were kept as no-flow boundaries throughout the experimentation. The water table was then lowered at incremental stages, allowed (approximately 60 min.) to equilibrate within the sand tank, and resurveyed along the same surface profile used in previous tests. The three water table levels selected for experimentation were designed to capture three specific moisture distribution conditions throughout the packed heterogeneous configurations. The first water table elevation was set at the top of the sand-pack to allow for ERT evaluations under fully saturated conditions. The second water table elevation was set at a vertical midpoint to allow for ERT evaluations under a transitional moisture content setting. The third and final water table elevation was set at a low point in the tank at approximately

20-30 cm. below our packed heterogeneous area of interest (i.e. the vertical intersection of coarse and fine layers). This experimental procedure of evaluating ERT methods under three distinct water table elevations was repeated for all three heterogeneous sand-pack configurations. See Figure 5.5 for photo of ERT equipment and moisture sensors installed in testing tank apparatus. For the duration of each sand tank experiment, water content and temperature were continuously monitored and recorded at five-minute intervals using self-contained data loggers.

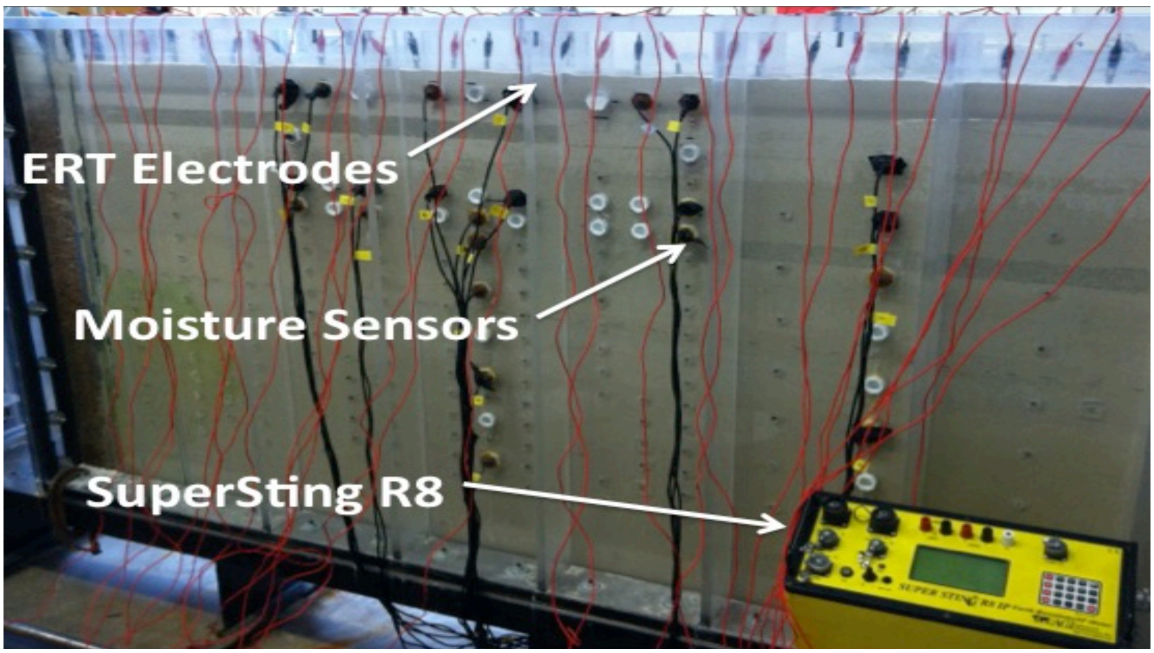

Figure 5.5. Photo of sand tank apparatus with ERT resistivity meter, moisture sensors, and electrode locations.

After performing the ERT sand tank evaluations and calibrating the moisture sensor data using the two-point α-mixing model, we then performed a series of soil gas diffusivity simulations using the water induced linear reduction model (WLR) [*Moldrup et al.*, 2000]. The water-induced linear reduction (WLR) model, used to estimate soil gas diffusivity, D_p/D_0 (where D_p is the soil gas diffusion coefficient [m^2s^{-1}/m^2s^{-1}] and D_0 is the gas diffusion coefficient [m^2s^{-1}/m^2s^{-1}] in free air), is based on traditional dry-soil models; however, it includes the effects of pore water blockage by including a parameter that captures relative soil air content. The general form of the WRL model is shown in

Equation 5.2:

$$\frac{D_p}{D_0} = \varepsilon^{X_{dry}} \left(\frac{\varepsilon}{\Phi} \right)^N \tag{5.2}$$

where ε is the soil air content ($m^3\ m^{-3}$) (obtained by using the observed saturation values and know sand properties), X_{dry} is a model parameter for pore tortuosity (1.33 used for this simulation as used by *Moldrup et al.*, [2000]), *N* is a model parameter that captures the water blockage (1.00 used for this simulation as used by *Moldrup et al.*, [2000]), and Φ is total porosity ($m^3\ m^{-3}$).

5.5 Proof-of-Principle Field Demonstration

The proof-of-principle field demonstration was conducted at an active VI site, seen in Figure 4.1, with a known dissolved-phase chlorinated solvent plume producing an observable VI signals. The field demonstration was performed using the same geophysical equipment (SuperSting RP8, Advanced Geosciences Inc.) and array configuration (Wenner) used in the laboratory experiments. A total of 28 electrodes (length = 60 cm, diameter = 1.75 cm) were used in each of the ERT surface profiles performed. The electrodes were made from similar stainless steel round bar-stock as were used in laboratory experiments, and were inserted directly into the soil surface. Three ERT surface profiles were established along intersecting transects for the duration of the field demonstrations, as seen in Figure 4.2.

Surface profiles #1, #2, and #3 were performed using an of an electrode spacing of 0.75 m., 1.5m, and 0.75 m., respectively, and spanned a total distance of 16 m., 30 m., and 16 m., respectively, as seen in Figure 5.6. We selected the electrode spacing based on an evaluation of the depth of investigation required (approximately 16 ft. bgs) and the spatial resolution needed to capture the fine sand stringers.

To collect moisture gradients in the shallow subsurface, five soil moisture sensors (ECH$_2$O EC-5, Decagon Devices Inc.), similar to those used in the laboratory experiments, were installed at depths of 0.25 m., 0.75 m., 1.25 m., 1.75 m., and 2.25 m. at the of the intersection of ERT *Profile #1* and *Profile #2*. Two temperature probes (EC-T,

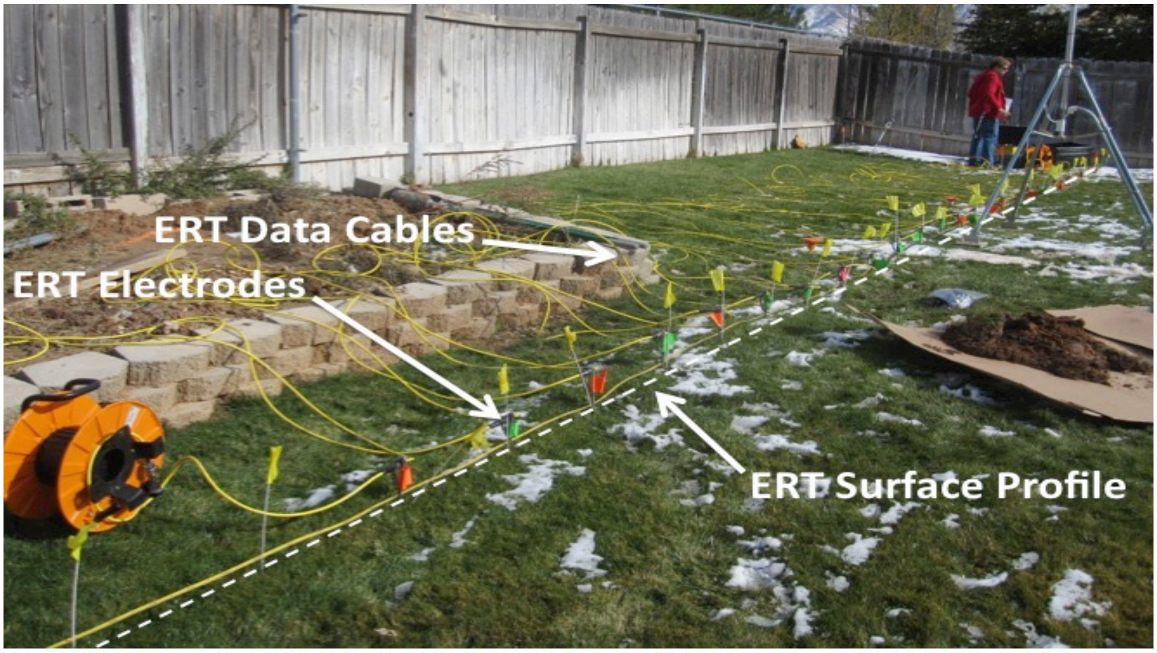

Figure 5.6. Photo of ERT surface profile being performed at field demonstration site.

Decagon Devices Inc.), similar to those used in the laboratory experiments, were installed at a depth of 0.75 m., and 2.25 m. at the same location. To install the soil moisture and temperature sensors, we excavated a hole to approximately 4 feet bgs using a commercially available post-hole digger and inserted the sensors directly into undisturbed soils along a vertical profile of the excavation sidewall. During the moisture and temperature sensor installation process we took caution to insert the sensors into undisturbed sections of soil because studies have shown that colleting moisture and temperature profiles in repacked soils can provide inconsistent values. The depth that we were able to install the soil moisture and temperature sensors was limited to the depth accessible when inserting the sensors by hand from the surface. For the duration of the field demonstration event, water content and temperature were continuously monitored and recorded at five-minute intervals by a self-contained, digital data logger (EM50, Decagon Devices Inc.) designed to power, read, and log data from compatible sensors. The soil moisture and temperature sensor data was later used to constrain the inversions of ERT data sets, as well as provide baseline profiles for soil moisture contents and temperatures. Once the moisture and temperature sensor networks were in place, initial ERT surveys along surface *Profiles #1, #2,* and *#3* were performed. The first series of surveys were designed to capture baseline geophysical profiles of the subsurface. To test our hypothesis, we then applied a moisture event to the surface (via a residential irrigation system) in an effort to simulate a natural precipitation event and resurveyed all three ERT profiles. Resurveying the ERT profiles after the induced moisture event allowed us to capture the temporal and spatial change in moisture distributions in response to the induced surface moisture event. To quantify to volume of water applied during the induced surface moisture event, we used metered rain gauges to collect and measure the water applied to the surface.

CHAPTER 6 – RESULTS AND DISCUSSION

The results presented in this section were collected from a series of laboratory experiments, performed in the CSM CESEP laboratory, and field demonstrations, performed at an active VI study site at Hill AFB, UT. Luke Shannon (CSM Civil and Environmental Department) performed laboratory experimentation. Luke Shannon and Brent Putman (CSM Geophysics Department) performed all field demonstrations. All ERT resistively data was modeled by Brent Putman.

6.1 Laboratory Experimentation

In this study, three heterogeneous sand-pack configurations were tested in a two-dimensional intermediate scale testing tank using a novel application of ERT to characterize VI pathway evolution. The experimental design utilized heterogeneous packing configurations and a variable water table in an effort to study fundamental REV-scale hydrologic processes that affect VI pathway evolution in unsaturated environments. I performed the ERT tests on three heterogeneous sand tank packing configurations, each one slightly more complex than the previous, in an effort to create a physical VI model that varied in complexity. During all stages of ERT sand tank experiments, soil moisture, temperature, and electrical conductivity were continuously monitored and used to constrain the ERT inversions and produce a series of qualitative soil gas diffusivity simulations. The observational results for soil moisture contents, soil gas diffusivity simulations, and ERT inversions were then compared against each other at three selected time steps (T_0, T_1, and T_2) to perform an evaluation of the performance of ERT in physical VI sand tank models.

Each packing configuration was tested using ERT under various selected water table elevations within the testing tank apparatus. Testing under several water table elevations was an important component in the experimental design because it allowed me to evaluate the performance of ERT under changing soil moisture content conditions.

Testing a potential VI characterization method over a wide range of soil moisture conditions is critical because moisture contents have been shown to have a pronounced affect on the evolution of VI pathways in the unsaturated zone [*Sakaki et al*, 2011]. For each packing configuration tested, the initial water table elevation was set at the top of the sand-pack. The second water table elevation was set at a mid-point within the sand-pack, creating partially saturated conditions in the regions above the water table. The final water table elevation was set at approximately 20-30 cm below the coarse layer, allowing for near residual saturation conditions to develop in the coarse horizontal channels.

During all stages of ERT testing, soil moisture contents were continuously monitored using soil moisture sensors (ECH$_2$O EC-5, Decagon Devices, Pullman, WA). The observed volumetric soil moisture contents are shown in Figure 6.1 (a-c). The results shown in Figure 6.1 (a-c) are presented at three selected time steps (T_0, T_1, and T_2), each capturing a unique soil moisture distribution stage within the testing tank. The first time step (T_0) shows the volumetric moisture content under full saturation conditions. Under these conditions, volumetric moisture content is equal to porosity. For the sands used during these tank experiments the total porosity values were 0.413 m^3/m^3, 0.330 m^3/m^3, 0.312 m^3/m^3, for #70 sand, #20/30 sand, and #12/20 sand, respectively (see Table 5.1 for additional sand properties). The second time step (T_1) shows the volumetric moisture content at an intermediate step, with the water table set at approximately 20 cm bgs and immediately below the coarse sand-packed layer. At this water table elevation, the upper most region of fine sands (#70) are still relatively close to saturation, with the volumetric moisture contents ranging from 0.243 m^3/m^3 in the shallowest zones monitored (approximately 4 cm bgs) to full saturation in the lower zones (well below the water table). At this time step, the volumetric moisture contents for the coarse sand layer (#20/30) are beginning to drain, with observed values of approximately 0.111 m^3/m^3. The final water table elevation, set at approximately 30 cm below the coarse packed layer, shows the coarse layer almost completely drained, with an observed saturation of 0.027 m^3/m^3. The fine packed layers, however, still contain a significant amount of water, with observed saturation values ranging from 0.185 m^3/m^3 in the shallowest regions (approximately 4 cm bgs) to full saturation, 0.413 m^3/m^3, at the lowest monitored regions (approximately 45-55 cm bgs). The contrast in volumetric moisture contents between the fine sand packed layers and the coarse sand packed layers becomes most pronounced at the lowest water table elevations, as seen by comparing Figure 6.1 (a-c) at time steps T_0 to time step T_2.

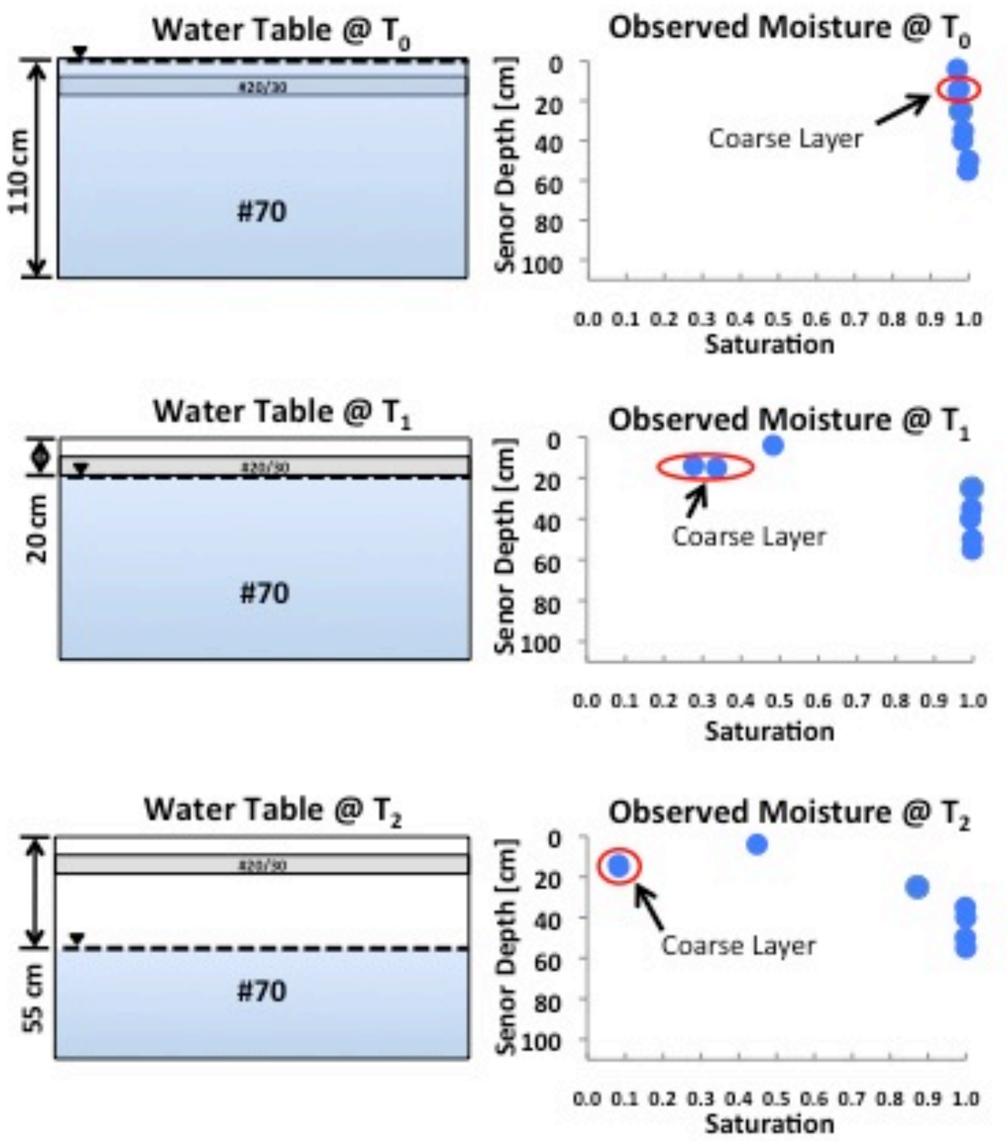

Figure 6.1 (a). Schematic of packing configuration #1 and the calibrated volumetric moisture content data [*e.g. Sakaki et al.*, 2008] with the water table set at the upper, mid and lower elevations (T_0, T_1, and T_2, respectively).

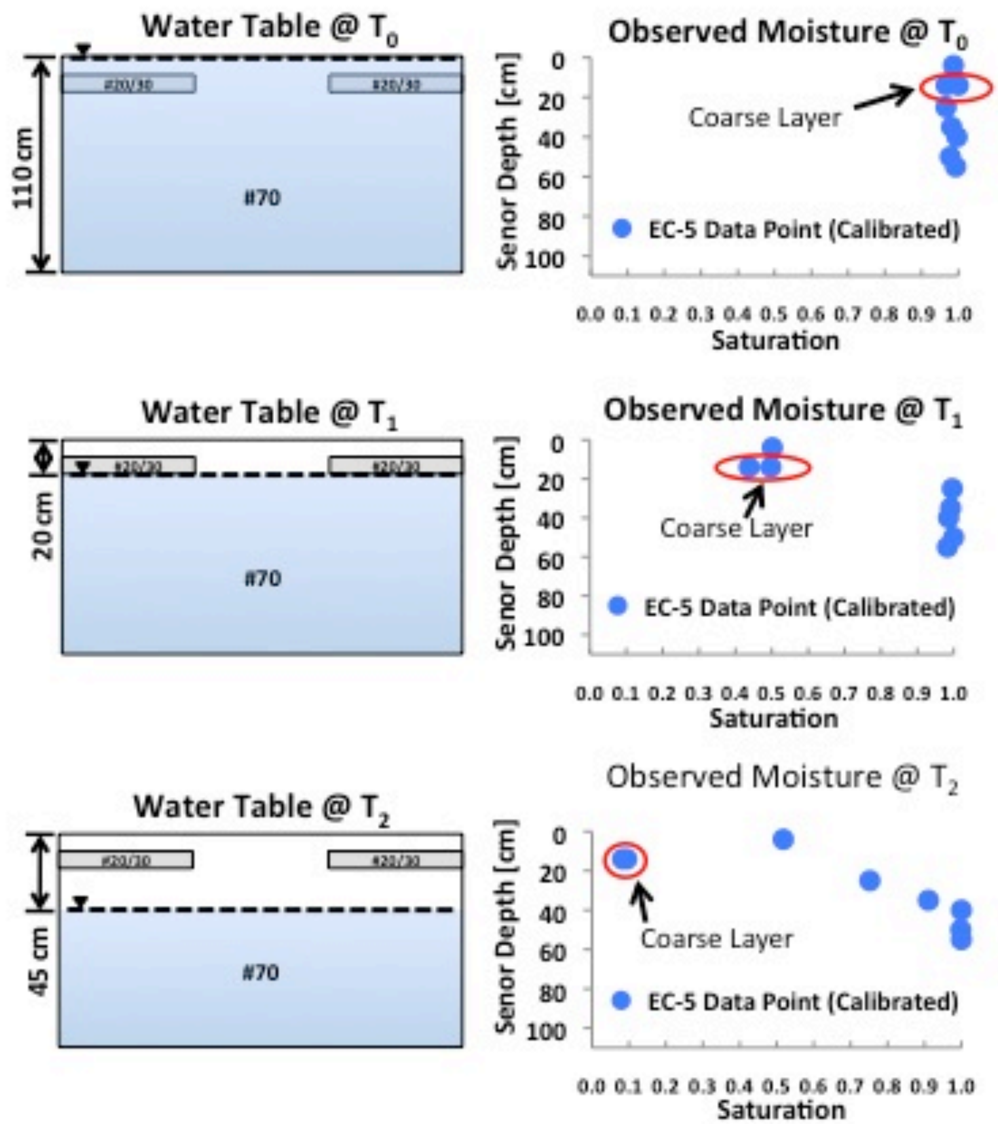

Figure 6.1 (b). Schematic of packing configuration #2 and the calibrated volumetric moisture content data [*e.g. Sakaki et al.*, 2008] with the water table set at the upper, mid and lower elevations (T_0, T_1, and T_2, respectively).

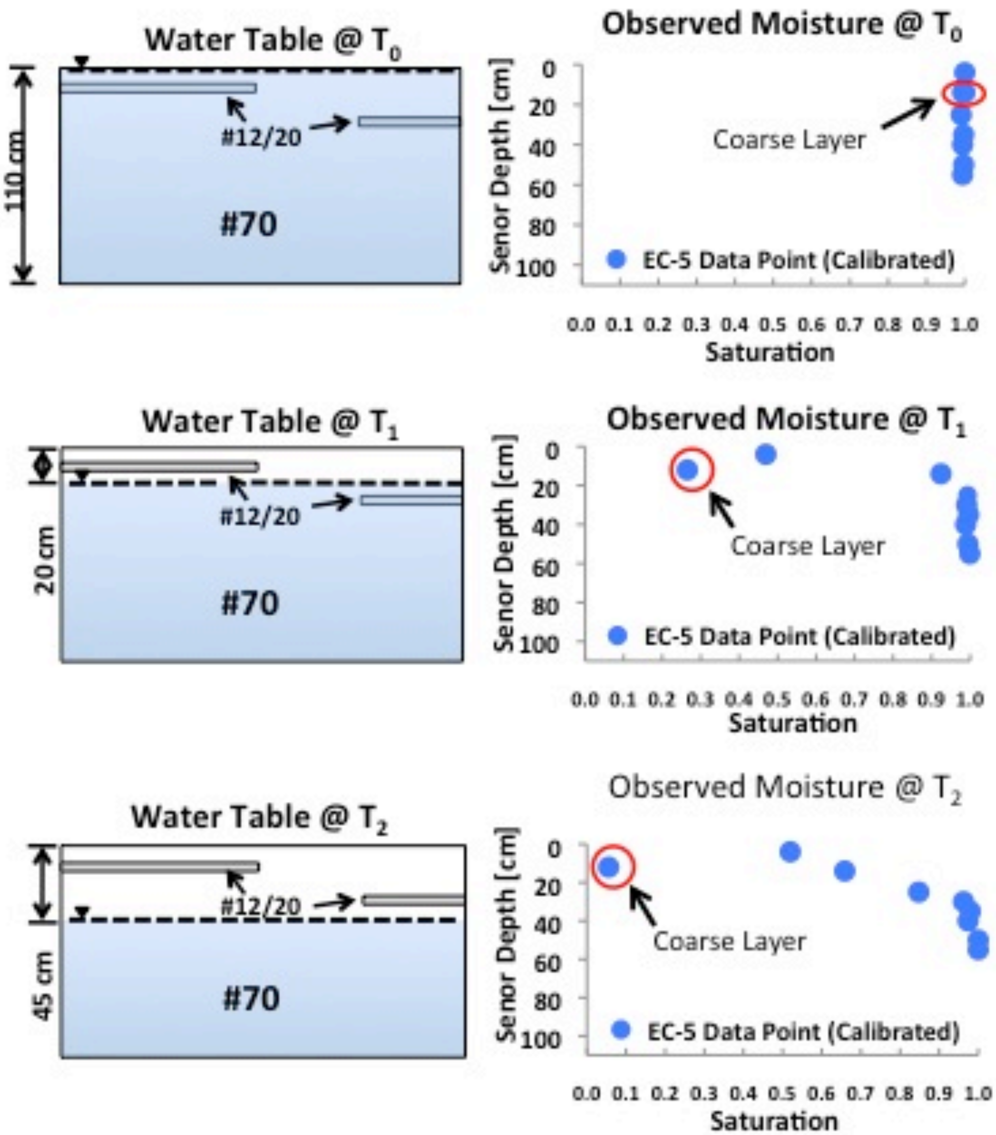

Figure 6.1 (c). Schematic of packing configuration #3 and the calibrated volumetric moisture content data [*e.g. Sakaki et al.*, 2008] with the water table set at the upper, mid and lower elevations (T_0, T_1, and T_2, respectively).

In an effort to examine the potential impact to VI pathway evolution that results from the strong volumetric moisture content contrasts between the coarse and fine sand layers in the testing tank, I used the experimentally observed moisture content values, along with know soil properties [*Smits et al.*, 2010], as input values for a water induced linear reduction (WLR) soil gas diffusivity model [*Moldrup et al*., 2000]. As no observation studies on soil gas diffusion were performed during these sand tank experiments, the WLR model simulations performed for this study cannot be validated and therefore should serve in a limited capacity as a qualitative evaluation tool for determining the performance of ERT VI characterization methodologies.

Figure 6.2 (a-c) shows the simulations of soil gas diffusivity rates through the two-dimensional testing tank, using the WLR model [*Moldrup et al*., 2000] at three selected time steps (T_0, T_1, and T_2), for packing configuration #1, configuration #2 and configuration #3, respectively. The color gradient for all diffusivity simulations represents soil gas diffusion rates in m^3/m^3; the red shaded regions are higher diffusivity rates and the blue shaded regions are lower diffusivity rates. The soil gas diffusivity simulations at time step T_0 are a simulation of the soil gas diffusivity with the water table at the top of the sand-pack. As no gas can pass through water-saturated soil pores, the simulated diffusivity rates for all packed sands at this time step (T_0) is zero, as indicated by the shaded blue regions in the figures. At time step T_1 the soil gas diffusivity simulations are produced with the water table set at a mid-point in the sand-pack, approximately 20 cm bgs. This time step shows the first initial stages of positive soil gas diffusivity rates developing in the testing tank. Based on an evaluation of the diffusivity simulations, only the coarse material develops the potential for positive gas diffusivity fluxes. The shaded white regions in the model simulations support this interpretation. At time step T_2 the soil gas diffusivity simulations are produced with the water table set at the lowest elevation in the sand-pack, at approximately 45-55 cm bgs. At this water table elevation, the simulated soil gas diffusivity rates reached the strongest contrast between the fine and coarse packed sands. In comparing the diffusivity simulation rates for packing configuration #1, #2 and #3 at time series T_2 the results indicate that packing configuration #3 does not develop as high a gas diffusivity rate as configuration #1 and configuration #2. This is likely due to the increased area of coarse material in configuration #1 and configuration #2. The dark blue shaded region that only develops in packing configuration #1 and #2 supports this model interpretation. It should also be noted that, effective diffusion rates for site-specific contaminants of concern (COCs) should also include the influence associated with temperature fluctuations and physical partitioning of the COCs due to soil sorption and water solubility.

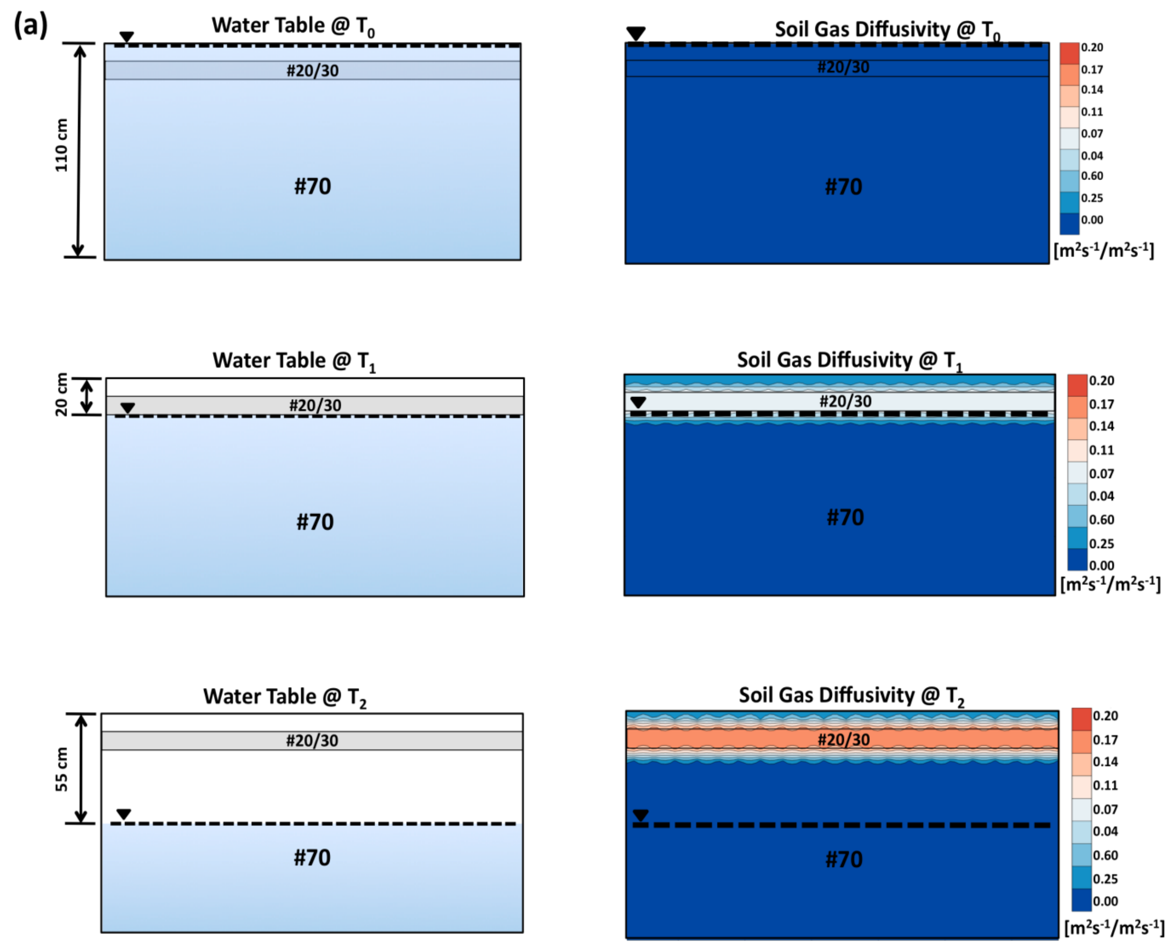

Figure 6.2 (a). Schematic of packing configuration #1 and the soil gas diffusivity simulations [*Moldrup et al.*, 2000] with the water table set at the upper, mid and lower elevations (T_0, T_1, and T_3, respectively).

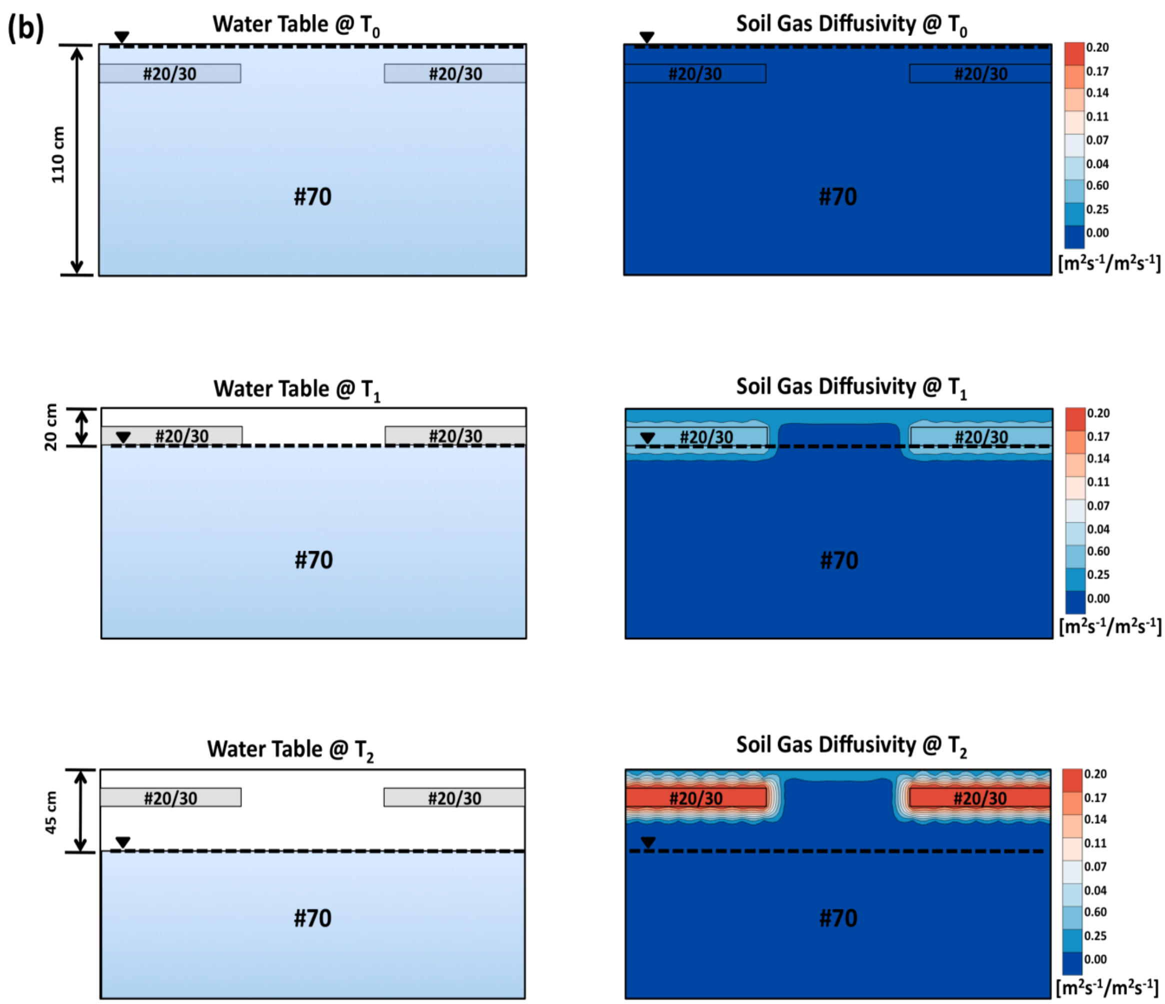

Figure 6.2 (b). Schematic of packing configuration #2 and the soil gas diffusivity simulations [*Moldrup et al.*, 2000] with the water table set at the upper, mid and lower elevations (T_0, T_1, and T_3, respectively).

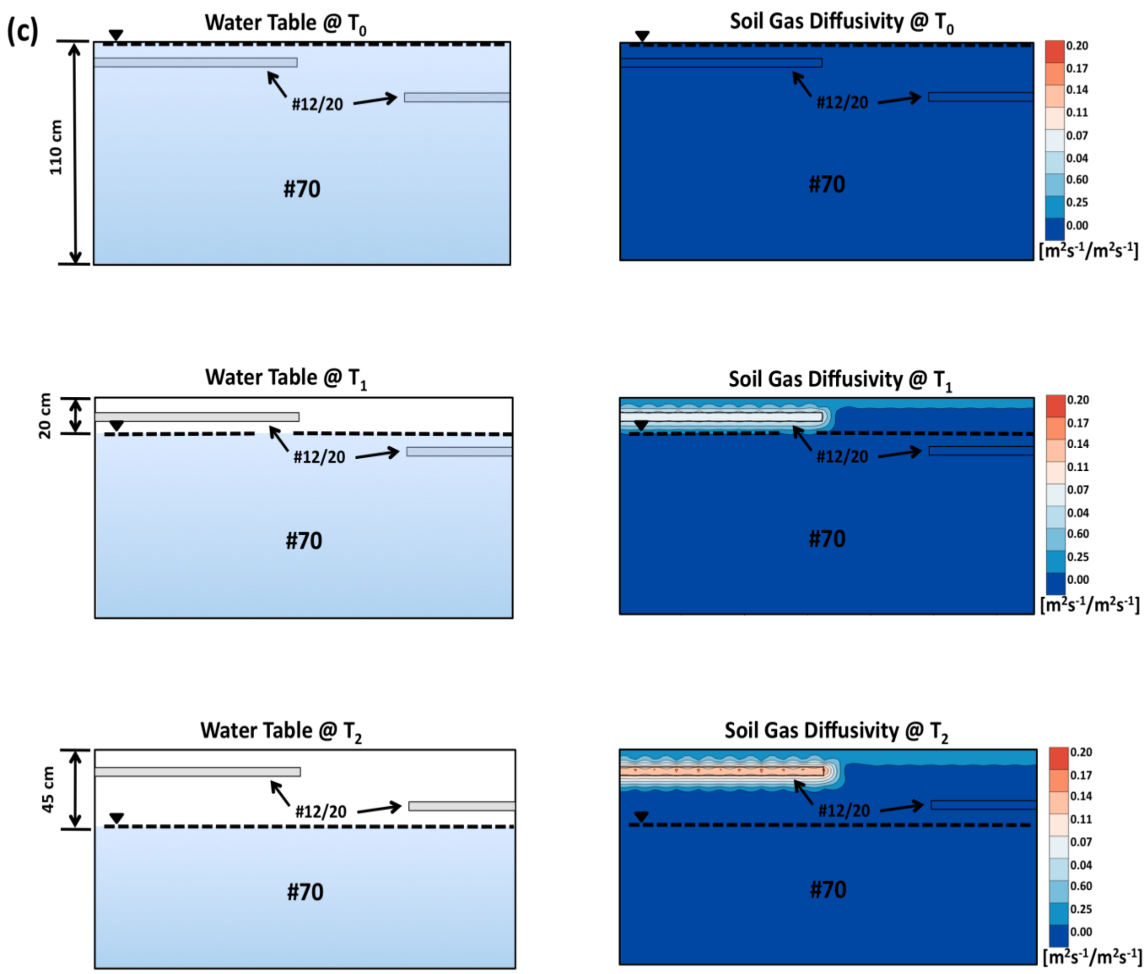

Figure 6.2 (c). Schematic of packing configuration #3 and the soil gas diffusivity simulations [*Moldrup et al.*, 2000] with the water table set at the upper, mid and lower elevations (T_0, T_1, and T_3, respectively).

The ERT resistivity inversion model results are shown in Figure 6.3 (a-c). All ERT resistivity inversion models results were produced by Brent Putman (CSM Geophysical Department, 2011-2012) using the University of British Columbia (UBC) Geophysical Inversion Facility (GIF) database model codes [*Oldenburg and Li*, 1994; *Li and Oldenburg*, 2000]. The ERT surveys were performed along surface profiles using a Wenner electrode array configuration. During all stages of ERT testing, volumetric moisture content, temperature, and electrical conductivity were continuously monitored and recorded via automated data loggers. These values (volumetric moisture content, temperature, and electrical conductivity) were then used to constrain the ERT inversion models. By using these observed experimental values in the constraint the ERT inversions, we were able to produce inversions that were theoretically closer representations of true subsurface conditions. The color gradients shown in Figure 6.3 (a-c) represent geoelectrical observations of the sand pack material by recording the resistance (in Ohm*m) in response to induced DC currents and performing inversions of the observed resistivity values. The blue shaded region indicates high resistance and the red shaded region represents low resistance or high conductance (also see color gradient key to right of ERT inversion cross sections).

In Figure 6.3 (a), at time step T_0, the upper region is shown with low levels of resistance, as indicated by the high amounts of shaded red area shown in the model domain. The lower resistance values are most likely associated with the higher amounts of pore space water, as water has a much higher conductance compared to the packed sands. However, this interpretation is not supported by the graphs shown in Figure 6.1 (a-c) that quantifies the volumetric moisture contents present in the sand pack material layers at each time step. Therefore, given the conceptual understanding that porous materials containing higher moisture contents (i.e. the fine sands in my sand pack) should theoretically pass electrical current much easier than porous materials containing lower moisture contents (i.e. the coarse sands in my sand pack) and using the moisture content values from Figure 6.1 (a-c) as a reference, the ERT inversions should reflect this contrast in moisture contents.

After close examination of the ERT inversion cross sections, there appears to be no consistent relationship seen in the inversions that capture the relative moisture contents associated with the fine versus coarse sand pack layers. The next time step, T_1, shown in Figure 6.3 (a-c), shows the ERT inversion cross sections with the water table at a mid-point. This time step does not capture the moisture distributions, as indicated by Figure 6.1 (b), or the fine versus coarse packed layers. The next time step, T_2, shown in Figure 6.3 (a-c) shows the ERT inversion cross-sections with the water table at the lowest elevation. This time step does not capture the moisture distributions, which are at the highest contrast levels, as indicated by Figure 6.1 (c), or the fine versus coarse packed layers.

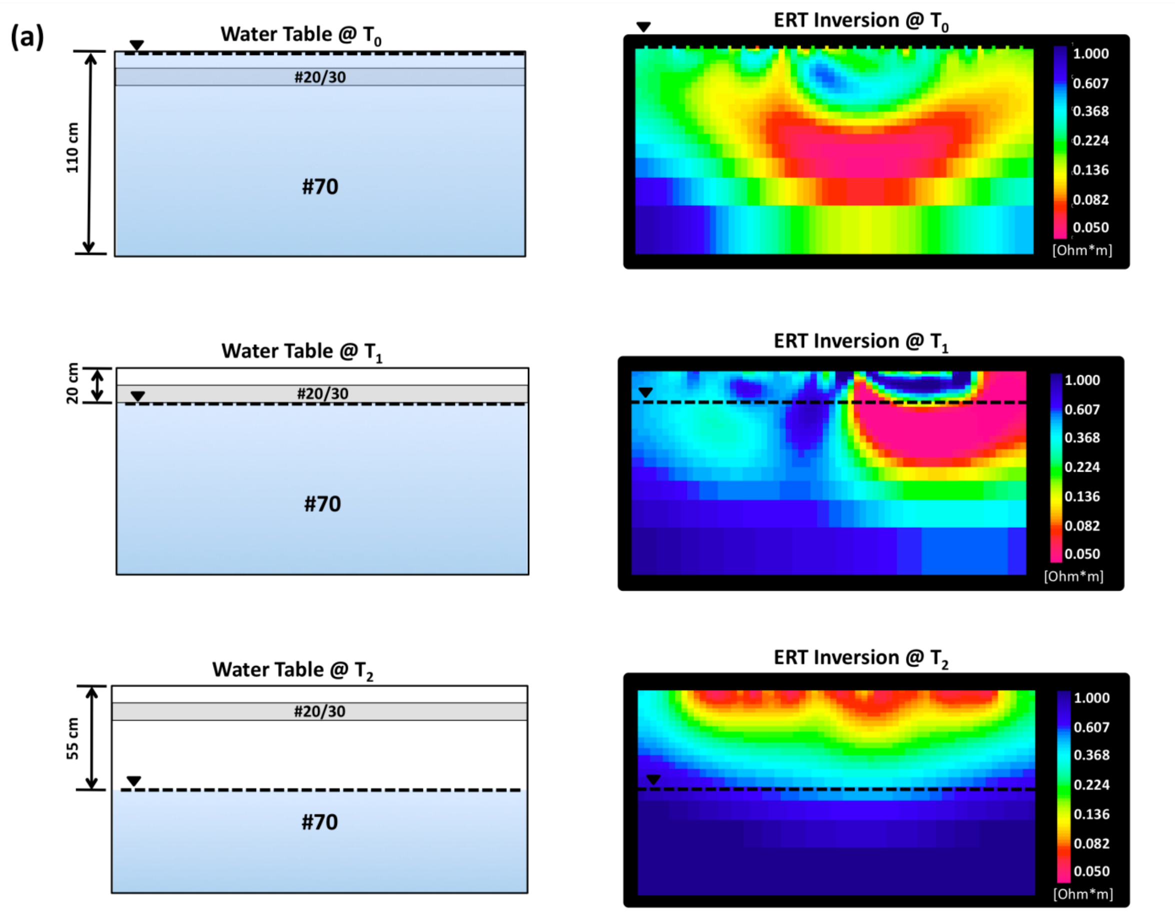

Figure 6.3 (a). Schematic of packing configuration #1 and the ERT inversions with the water table set at the upper, mid and lower elevations (T_0, T_1, and T_3, respectively). The ERT inversion color gradients represent resistivity values with ranges from 0.05 Ohm*m to 1.00 Ohm*m. All ERT inversions were performed by *Brent Putman* from the CSM Geophysics Department, [2011-2012].

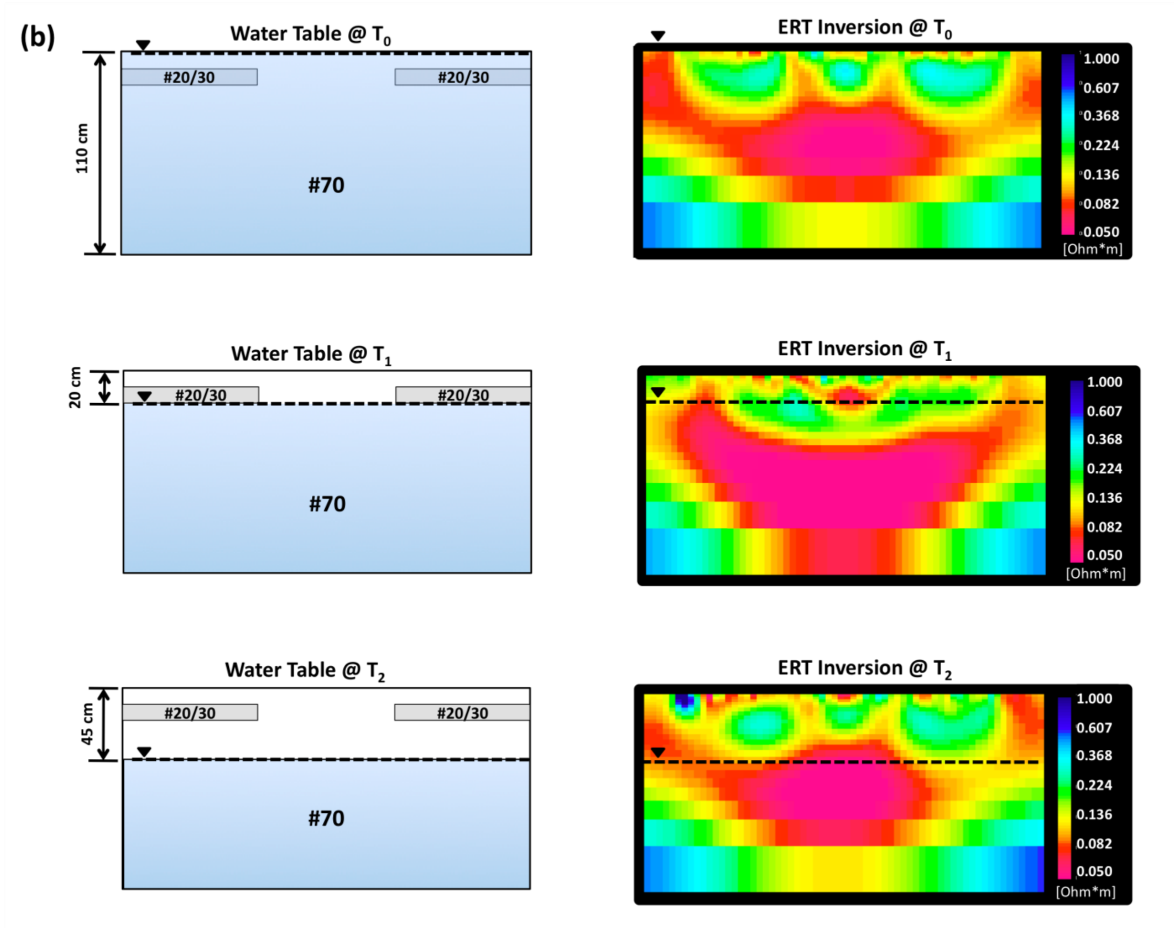

Figure 6.3 (b). Schematic of packing configuration #2 and the ERT inversions with the water table set at the upper, mid and lower elevations (T_0, T_1, and T_3, respectively). The ERT inversion color gradients represent resistivity values with ranges from 0.05 Ohm*m to 1.00 Ohm*m. All ERT inversions were performed by *Brent Putman* from the CSM Geophysics Department, [2011-2012].

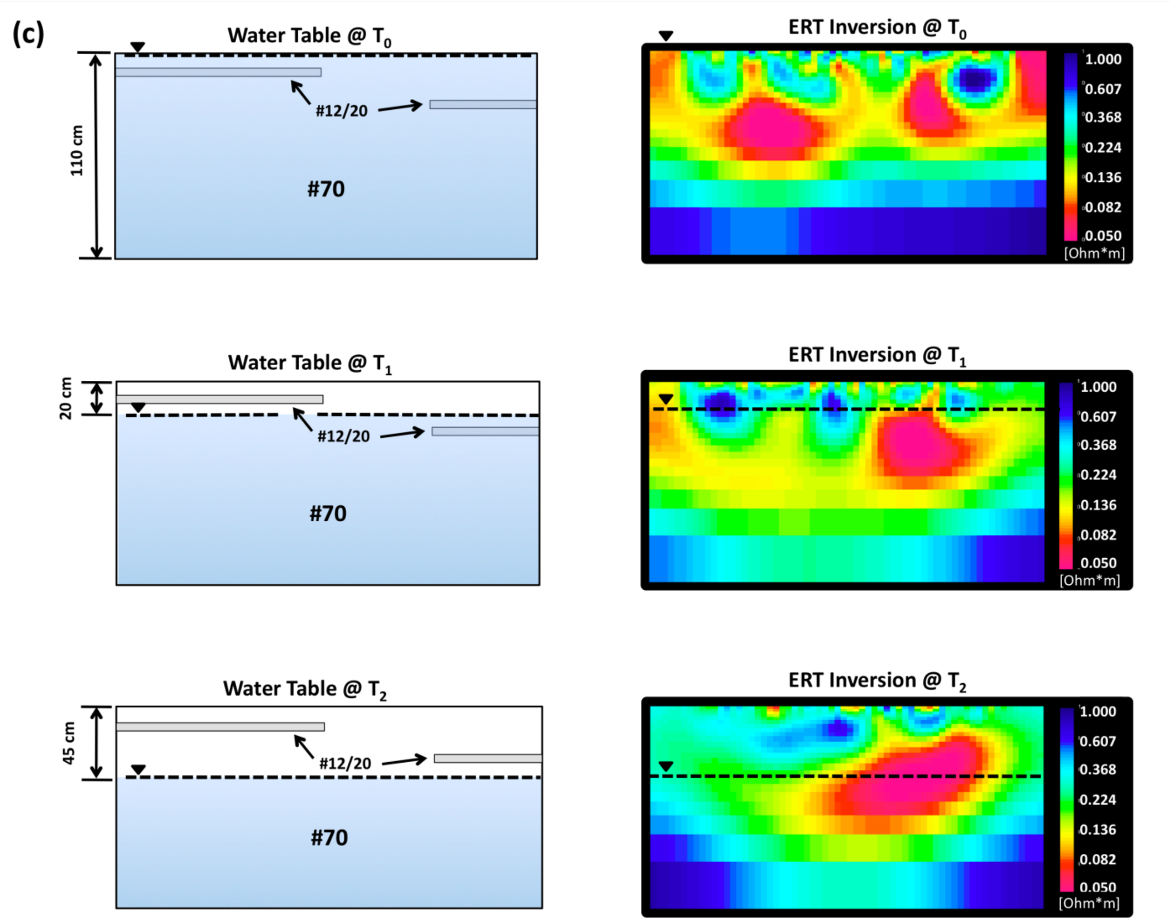

Figure 6.3 (c). Schematic of packing configuration #3 and the ERT inversions with the water table set at the upper, mid and lower elevations (T_0, T_1, and T_3, respectively). The ERT inversion color gradients represent resistivity values with ranges from 0.05 Ohm*m to 1.00 Ohm*m. All ERT inversions were performed by *Brent Putman* from the CSM Geophysics Department, [2011-2012].

6.2 Field Demonstration

The field demonstration was performed to serve as a proof-of-concept evaluation of the practical application of ERT for VI characterization at VI field sites. The approach was based on providing a qualitative evaluation of the ERT VI characterization methodologies developed in the laboratory ERT sand tank tests. The general experimental design of our field demonstration was based on the concept of inducing a disturbance (via a simulated precipitation event) in the unsaturated zone that would create an observable change in the VI signal entering the building. By using an induced surface moisture event I was able to successfully observe the response in the system using both soft geophysical methods and hard analytical methods. By creating a simulated precipitation event that was observable in both the analytic data and the geophysical ERT data, we were able to develop a joint-interpretation of the hard and soft data associated with induced perturbation in the VI signal.

Using data available from an onsite Meteorological Station (MET) station [*Ongoing VI site study by Johnson et al.*, 2010-2012], I was able to statistically analyze all local precipitation events over the previous 16 months and determine an appropriate volume of water to release on the surface during the induced moisture event. The observed MET station data is shown in Figure 6.4 (a) and the statistical analysis is shown in Figure 6.4 (b).

Using statistical analysis of local precipitation events to create a Boxplot of the precipitation data collected on-site over the past 16 months, seen in Figure 6.4 (a) and (b), we were able to recreate a moisture event (using the residential sprinkler system available on-site) that was volumetrically proportional to the largest 10-percentile precipitation events (approximately 1.8 - 2.5 cm). The Boxplot, seen in Figure 6.4 (b), quantifies the mean 50-percentile (indicated by the boxed region in the plot) and the upper and lower 25-percontile data points (identified by the upper and lower whisker regions in the plot). To quantify the volume of water absorbed by the ground surface, moisture and temperature sensors were installed (at approximately 1 ft bgs) in undisturbed soils directly adjacent to ERT profiles. In addition, several rain gauges were placed along the surface profiles to record the volumes released. By combining the historical statistical analysis with observed induced precipitation data, we were able to validate to volume of water applied to the ground surface during our ERT field demonstration. Validating the volume of water applied to the ground surface was important because the results from this study could potentially be used by residential home owners to make more informed decisions about the potential for inducing VI into their homes based on when and how much water they apply during irrigation. Additionally, the result from this study may also be used for future regulatory screening standards.

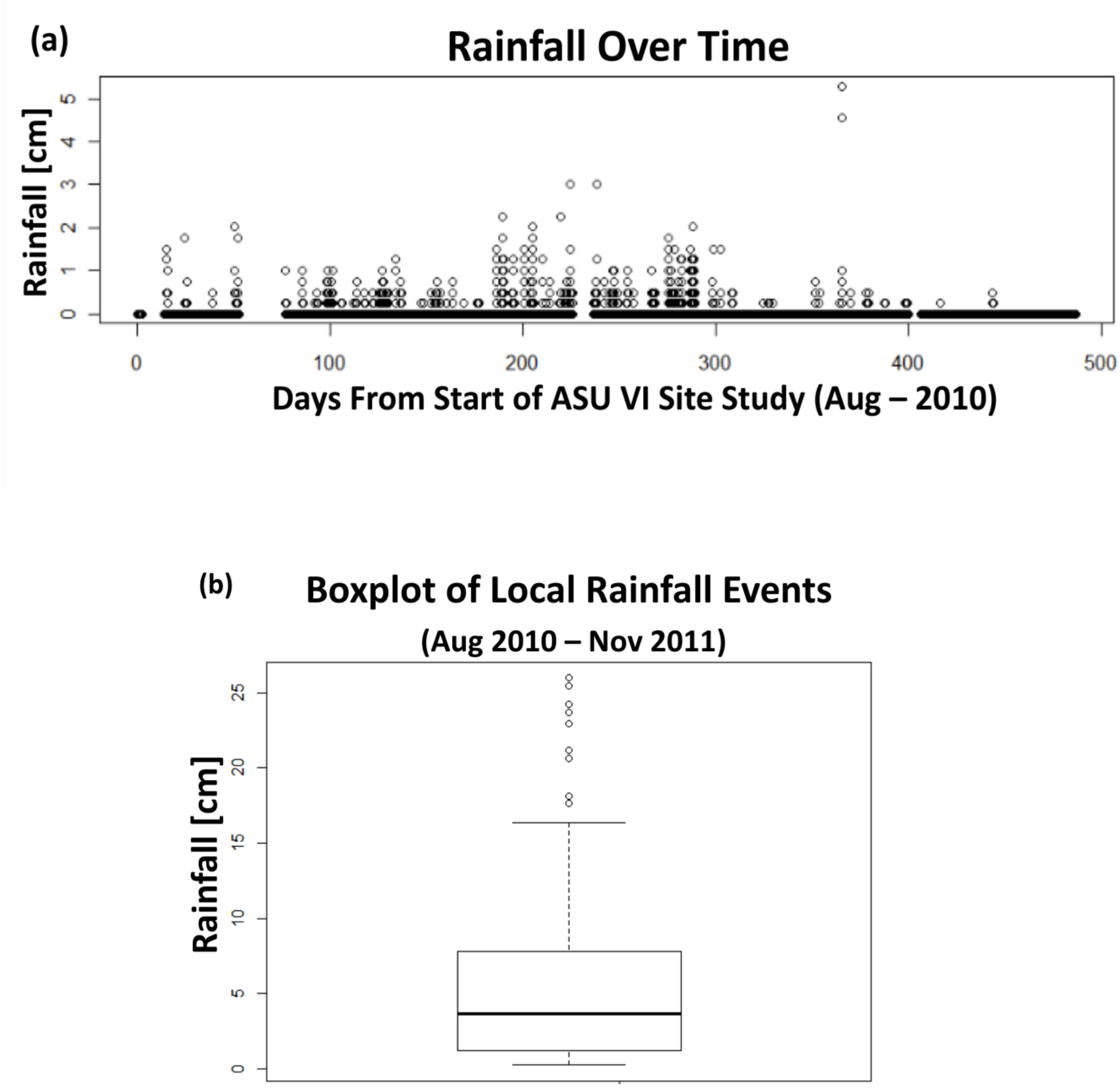

Figure 6.4 (a) and (b). (a) MET station precipitation data from field site and (b) Statistical analysis of local precipitation events from field site.

Figure 6.5 shows temperature and volumetric moisture changes in the unsaturated zone (at approximately 1 ft bgs) immediately before, during, and after the simulated precipitation event. The general hypothesis driving the experimental approach of our field demonstration was the prediction that, at REV-scales, wetting fronts migrate vertically downward, producing a compression effect on the VI channels, which in turn create an associated spike in VI concentrations entering the building. Additionally, if enough water volume is present in the wetting front, VI channels in the unsaturated zone can potentially be cut-off altogether as a result of complete displacement soil pore-space air with the infiltrating water. For this field demonstration, ERT was used to capture the induced moisture event, the associated wetting front, and lateral migration into active coarse VI channels.

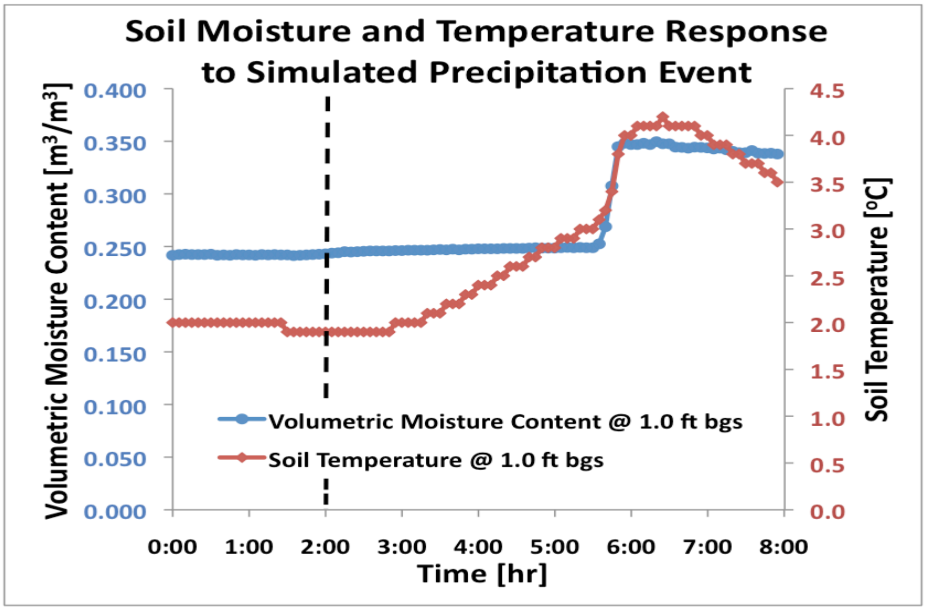

Figure 6.5. Temperature and volumetric moisture content changes in response to simulated moisture event.

Figure 6.6 (a-d) shows time-series snap shots of ERT inversions before, immediately after, and approximately 2 and 4 hours after the induced precipitation event. (Please note, due to an equipment operator error in which the SuperSting hard drive was inadvertently reformatted resulted in the loss of the initial {T_0} ERT inversion data files. The initial ERT inversion {@ T_0} that is used in Figure 6.6 {a} is a profile captured along the exact same spatial profile as the inversions used in Figure 6.6 {b-d}, however, it was collected during a site visit in November of 2011, approximately 5 months earlier. This is also the reason the resistivity scale is different for Figure 6.6 {a} as compared to the later time steps). The scale used in Figure 6.6 (a-d) is Ohm*m, with the blue shaded regions representing material with high electrical resistivity and the red shaded regions representing the lower electrical resistivity values. The white crosshatched region, seen along the lower sections of Figure 6.6 (a-d), represent regions of the model domain where the model predictions are no longer reliable. The depth of investigation (indicated by the colored region in the model domain) is approximately 6-7 m. bgs. By comparing the inversions seen in Figure 6.6 (a), at time step T_0, to the inversions seen in Figure 6.6 (b-d), at time step T_1, T_2, and T_3, respectively, we can observe the change in geoelectrical properties associated with the water introduced during the simulated precipitation event. This is seen in the inversions by a slight decrease in the concentration of the red shaded region along the ground surface, especially on the left sides of the cross section where the surface elevation is lower. At the initial time step (T_0), a potential boundary layer can also been seen at approximately 2 m. bgs. This interpretation is supported by the sharp contrast in geoelectrical properties (and corresponding color gradients) at approximately 2 m depth that appear to be horizontally (relative to ground surface) continuous in the inversions. At later time steps ($T_1 – T_3$), the higher resistive regions (indicated by the blue shaded region) below the potential boundary layer begin to become infiltrated with the water induced from the simulated precipitation event and the upper regions begin to drain out. This interpretation is supported by closely evaluating the geoelectrical changes, indicated by the transitional steps from dark blue to light blue, seen in the regions below the boundary layer in time-series T_1, T_2, and T_3, respectively. The inversions also show that the wetting front does not infiltrate evenly throughout the horizontal (relative to ground surface) profile captured in our ERT resistivity data. The wetting front appears to preferentially infiltrate along the left side of the inversion cross sections and indicate a lateral infiltration up gradient, as seen in Figure 6.6 (b) and (c).

By capturing time-series snap shot profiles of the vadose zone in response to the simulated moisture event using ERT, we were able to successfully distinguish the wetting front infiltrating the unsaturated zone, capture a region of lateral infiltration, and develop a joint-interpretation using both hard and soft data. The observation in the ERT inversions of lateral infiltration between T_0, T_1, and T_2 temporally coincides with a spike in the VI signal observed in the study site building using a GC/MS. The VI signal data, collected by the ASU research group [*Ongoing VI site study by Johnson et al.*, 2010-2012] provided the hard VI data used to spatially and temporally constrain the infiltrating water's impact to the vapor pathways. By combining these soft and hard data sets, I have demonstrated a novel joint-interpretation of ERT data with GC/MS data and have developed a more comprehensive conceptual site model of the location of VI pathways in the subsurface surrounding a VI impacted building.

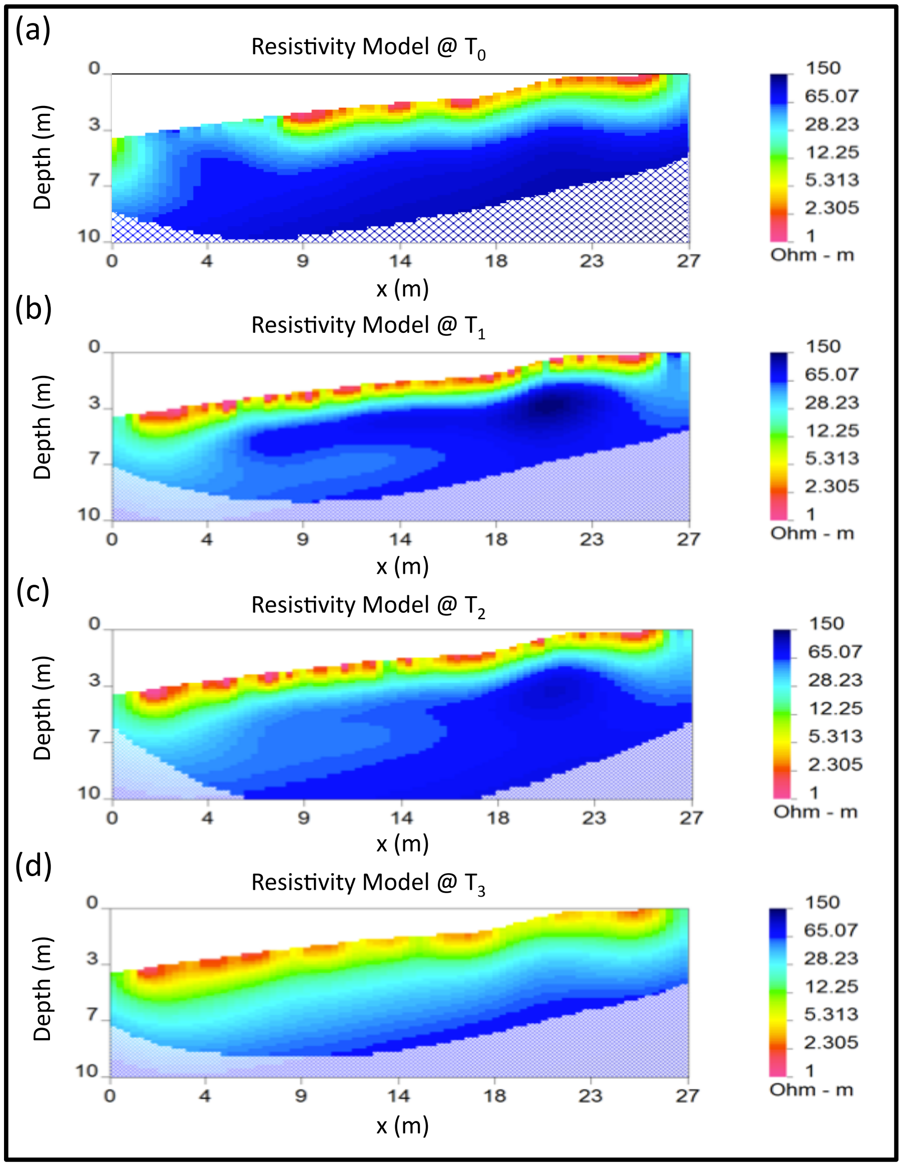

Figure 6.6. Time series snap shots of ERT surveys capturing initial site conditions and the infiltrating wetting front induced by our simulated precipitation event.

Figure 6.7 shows the Hapsite GC/MS readings over a five-day window that captured our simulated precipitation event and the response in the VI signal. As shown on Figure 6.7, the VI signal over the previous four days showed no positive values from approximately 6:00AM in the morning till 12:00AM midnight. This diurnal cycle is likely a result of the pressure differentials created by nightly use of a central heating unit. The use a central heating unit results in decreased interior pressures due a chimney effect developing inside the building as the heat rises and exits through the roof. After performing the simulated precipitation event, we observed a mid-day spike in TCE, at approximately 0.044 ppbv, from a portable on-site gas chromatograph and mass spectrometer (Hapsite GC/MS ER, Inficon, Syracuse, New York). By observing this potential impact in the VI signal in response to our simulated precipitation event, we were able to develop a novel joint-interpretation using the soft geophysical data, produced by ERT resistivity inversions, and the hard analytic data, produced from the onsite GC/MS unit. Combining these hard and soft data sets allowed for the prediction that the water infiltrated coarse VI channels that forced the VI signal to spike as the air was displaced by infiltrating water.

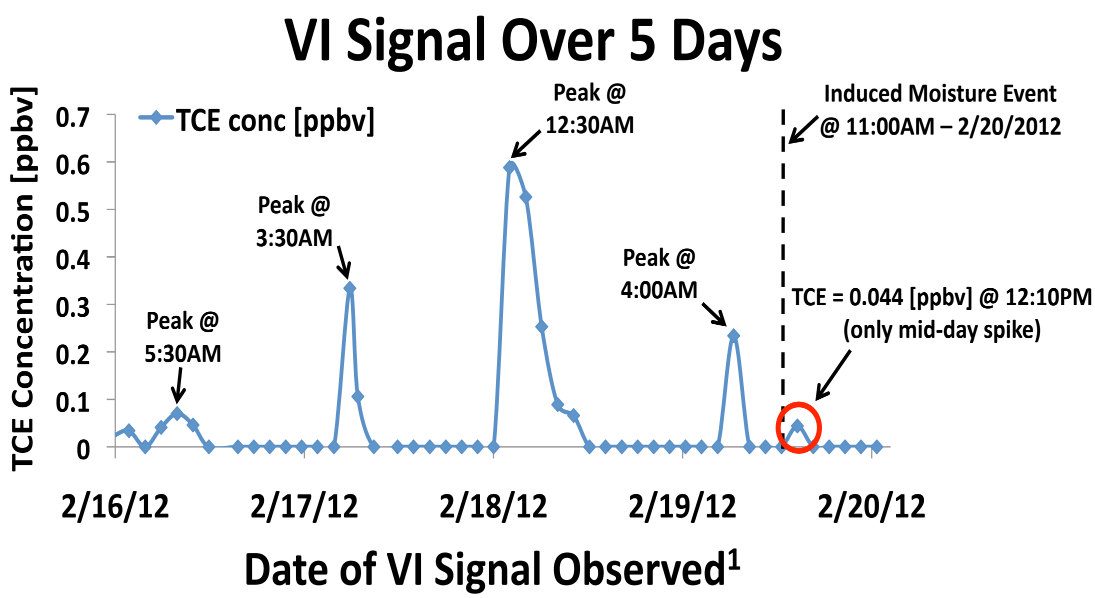

Figure 6.7. Graph of the VI signal (TCE in ppbv) entering study site building over a five-day window that included our field demonstration and simulated precipitation event. [*Ongoing VI site study by Johnson et al.*, 2010-2012].

Figure 6.8 shows a conceptual diagram of the joint-interpretation method used through temporally overlapping the soft and hard observational methods. This figure helps visual conceptualize the joint-interpretation method used and how the data sets temporally relate. Performing the joint-interpretation of hard and soft observational methods allowed me to constrain the spatial regions in the vadose zone surrounding the house where preferential VI channels likely exist. For our specific field demonstration site, the joint-interpretation indicates that the front yard in the southeast corner of the residential lot most likely contains preferential VI pathways.

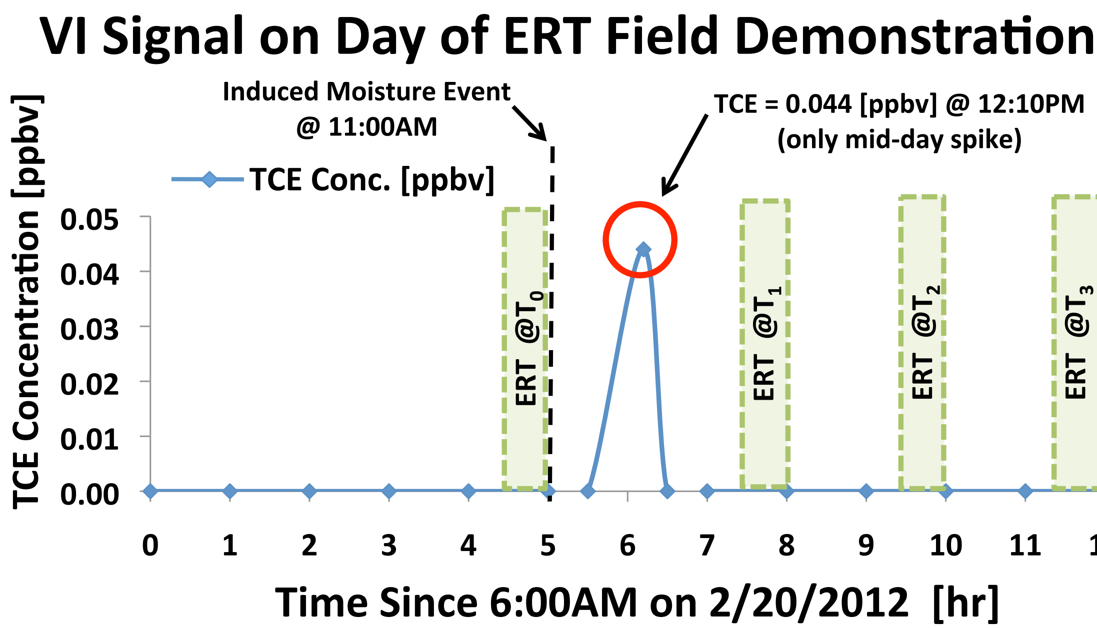

Figure 6.8. Graph of the VI signal (TCE in ppbv) entering study site building over 1-day window during our ERT field demonstration with ERT time-series snap shots overlaid on the VI signal timeline [*Ongoing VI site study by Johnson et al.*, 2010-2012].

CHAPTER 7 – DISCUSSION AND CONCLUSION

The research performed in this study investigated a novel application of ERT for VI site characterization in the unsaturated zone. Improving current VI site characterization methods is important because VI can carry harmful VOCs or radioactive particles into buildings, often causing indoor air quality to drop below minimum health standards [*Johnson and Ettinger*, 1991]. Geophysical methods such as ERT hold the potential to greatly improve our spatial and temporal data sets related to VI site characterization. By developing new methods to collect these data sets, tools such as predictive VI models can be improved. Applying ERT to VI site characterization can help improve current predictive VI models by providing additional data, allowing site managers to build a more comprehensive conceptual site model of VI pathways in the unsaturated zone.

This study was driven by three research questions that outlined key VI-related parameters that our ERT laboratory scale tests and ERT field scale demonstration focused on capturing. *Research Question #1* addressed the ability of ERT to distinguish relative soil moisture distributions and lithologic compositions in heterogeneous soil formations, thus identifying potential preferential VI pathways. This was evaluated by performing a series of intermediate scale two-dimensional ERT sand tank tests using heterogeneous packing configurations under a range of saturation conditions. During the laboratory experiments, soil moisture, temperature, and electrical conductivity were continuously monitored; the data was used to constrain the ERT inversion models as well as produce a series of qualitative soil gas diffusivity simulations. Based on the ERT inversion cross sections, our initial evaluation of the potential application of ERT for VI site characterization is promising and warrants further investigation. Although the model produced by our ERT resistivity data did not successfully characterize relative soil moisture distributions or lithologic compositions in our testing tank apparatus, a common electrical source of error may resolve the model performance. All three sand tank configurations tested using ERT produced similar inaccuracies in the model results. As the observed resistivity values were an order of magnitude lower than the modeled values, the inaccuracies were likely a three-dimensional artifact created as a result of electrical sinks present in the testing tank apparatus. The electrical sinks were most likely associated with current leakage through electrical wires or steel mesh screens present in the testing tank apparatus.

Future ERT laboratory experiments will address the sand tank design flaw by focusing on resolving the electrical sink issue. I will address these potential sources of error by removing all objects that conduct electricity and may contribute to the electrical sinks. This includes removing metal mesh screens built into the testing tank, sensors with electrical leads running out of the tank, and carefully examining the tank for water leaks. After resolving the electrical sink issue I will rerun the previous sand pack configurations and reevaluate how well ERT can distinguish relative moisture contents and lithologic compositions. Final sand tank experiments should attempt to fully test the range of ERT in distinguishing thin coarse layers.

Research Question #2 addressed the feasibility of ERT as a practical tool for VI characterization in a field environment. This was investigated by performing a field demonstration using ERT at an active VI site near Hill AFB, UT, U.S.A. The technical approach used for our field demonstration was to induce a surface moisture event (using a residential sprinkler system) at the VI site and monitor the response in vadose zone moisture redistributions using ERT while simultaneously monitoring the VI signal response (to the same surface moisture event) using an on-site gas chromatograph/mass spectrometer (GC/MS) located inside the study site building. Results demonstrated that ERT can capture soil moisture migration through preferential pathways in the subsurface, demonstrating that ERT can be used to provide valuable spatial and temporal information about the soil moisture and lithology of the subsurface. . Evaluating the ERT inversions over time provides a mechanism to spatially constrain a region of the subsurface where preferential VI pathways likely exist. Comparing ERT data and GC/MS data demonstrated that the wetting event may have induced the transport of TCE? into the building. However, these results are preliminary and additional testing is needed. The successful demonstration of ERT to an active VI site demonstrates that the proper interpretation of ERT data can aid site managers in developing more comprehensive VI pathway conceptual site models.

Future work evaluating ERT as a VI site characterization tool should focus on determining the full potential range of ERT for VI site characterization applications. This will include increasing the number of electrodes, while maintaining the same total depth of penetration, to provide better resolution of both soil moisture contents and lithologic composition. The ERT unit (SuperSting R8/IP Earth Resistivity Meter, AGI, USA) used in these experiments can accommodate up to 65,000 electrodes at once; we used 28 electrodes. By increasing the number of electrodes used, we would also be improving the resolution of our inversions and potentially capture previously undetected contrasts in moisture content and lithology. Additionally, future tests should perform a series of field demonstrations, rather than only one or two, to allow for a better evaluation of the repeatability of data.

By characterizing key VI parameters such as pore moisture content and lithologic compositions, geophysical methods such as ERT can potentially provide high-resolution data sets that far surpass traditional point-sampling methods. Observing and monitoring VI pathways using soft imaging techniques such as ERT *and* hard analytical methods such as GC/MS, allows for the joint-interpretation of hard and soft data to develop a more comprehensive conceptual site model of preferential VI pathways in the unsaturated zone. This improved conceptual VI site model can be used to aid environmental site managers in developing risk assessments and remediation approaches for VI sites.

REFERENCES CITED

Abreu L.D.V., Johnson P.C. 2005. Effect of vapor source – building separation and building construction on soil vapor intrusion as studied with a three-dimensional numerical model. *Environ. Sci. Technol*. (39): 4550-4561.

Aizebeokhai A.P., Olayinka Al., Singh V.S. 2009. Numerical evaluation of 3D geoelectrical resistivity imaging for environmental and engineering investigations using orthogonal 2D profiles. *SEG Expanded Abstracts 28*, 1440: 1440-1444, DOI:10.1190/1.3255120.

Aizebeokhai A.P., Olayinka Al., Singh V.S. 2010. Application of 2D and 3D geoelectrical resistivity imaging for engineering site investigation in a crystalline basement terrain, southwestern Nigeria. *Journ. Environ. Earth Scien*. DOI: 10.1007/s12665-010-0474-z, p. 1481.

Amidu S. A., Olayinka Al. 2006. Environmental assessment of sewage disposal systems using 2-D electrical resistivity imaging and geochemical analysis: A case study from Ibadan, Southwestern Nigeria. *Environ. Eng. Geosci*. 7(3):261-272.

Baehr A.L. Stackelberg P.E. Baker R.J. 1999. Evaluation of the atmosphere as a source of volatile organic compounds in shallow groundwater. *Water Resour. Res.* (35): 127-136.

Brunet P., Clement R., Bouvier C. 2010. Monitoring soil water content and deficit using electrical resistivity tomography (ERT) – A case study in the Cevennes area, France. *J. of Hydrology*. 380(1-2): 146-153.

Christophersen M., Broholm M.M., Mosbaek H., Karapanagoiti H.K., Burganos V.N., Kjeldsen P. 2005. Transport of hydrocarbons from an enplaced fuel source experiment in the vadose zone at Airbase Vaerlose, Denmark. *J. of Contam. Hydrol*. (81): 1-33.

Dahlin T., Loke M.H. 1997. Quasi-3D imaging-mapping of three-dimensional structures using two-dimensional DC resistivity techniques. *Proceedings of the 3rd Meeting of the Environ. Eng. Geophy. Soc.*: 143-146.

Darby S., Hill D., Auvinen A., Barrios-Dios J.M., Baysson H., Bochicchio F., Deo H., Falk R., Forastiere F., Hakama M., Heid I., Muirhead C., Oberaigner W., Pershagen G., Ruano-Ravina A., Ruosteenoja E., Rosario A.S., Tirmarche M., Tomasek L., Whitley E., Whichmann H.E., Doll R. 2005. Radon in homes and risk of lung cancer: collaborative analysis of individual data form 13 European case-control studies. *Br. Med. J.* (330): 223-226.

Daily W., Ramirez A., LaBrecque D., Barber W. 1995. Electrical resistance tomography experiments at the Oregon Graduate Institute. *J. of App. Geophy*. (33): 227-237.

Fitzpatrick N.A., Fitzgerald J.J. 2002. An evaluation of vapor intrusion into buildings through a study of field data. *Soil and Sed. Cont.* 11(4): 603-623.

Franz T. E., Nolan J., Nordbotten J.M., Caylor K. K., Slater L.D. 2010. Quantifying transient soil moisture dynamics using multipoint direct-current resistivity in homogeneous sand. *Vadose Zone J.* (10): 286-298.

Garbesi K., Sextro R.G. 1989. Modeling and field evidence of pressure-driven entry of soil gas into a house through permeable below-grade walls. *Environ. Sci. and Technol*. 23 (12): 1481-1487.

Griffiths D.H., Barker R.D. 1993. Two dimensional resistivity imaging and modeling in areas of complex geology. *J. Appl. Geophy.* 29: 211-226.

Griffiths D.H., Turnbull J, Olayinka Al. 1990. Two-dimensional resistivity mapping with a complex controlled array. *First Break*, 8: 121-129.

Hers I., Atwater J., Li I., Zapf-Gilje R. 2000. Evaluation of vadose zone biodegradation of BTX vapours. *J. of Contam. Hydrol*. 46: 233-264.

Johnson P.C., Ettinger R.A. 1991. Heuristic model for predicting the intrusion rate of contaminant vapors into buildings. *Env. Sci. and Tech.* 25 (8): 1445-1452.

Johnson P.C., Luo H., Holton C. 2010-2012. Ongoing VI site study. Hill AFB, Layton, UT, U.S.A.

Jury W.A., Russo D., Streile G., Abd. H.E. 1990. Evaluation of volatization by organic chemicals residing below the soil surface. *Water Resources Reseach.* 26(1): 13-20.

Keskikuru T., Kokotti H., Lammi S., Kalliokiski P. 2001. Effect of various factors on the rate of radon entry into two different types of houses. *Building Environ*. (36): 1091-1098.

Kunetz G. 1966. Principals of Direct Current Resistivity Prospecting. *Gebruder Bomtraeger*, Berlin, p.103.

Li, Y. and Oldenburg, D. W. 2000. 3D inversion of induced polarization data, *Geophysics.* (65): 1931-1945.

Liu N. 2007. Soil and Site Characterization Using Electromagnetic Waves, PhD. Thesis, Virginia Polytechnic Institute and State University.

Michot D. et al. 2003. Spatial and temporal monitoring of soil water content with an irrigated corn crop cover using surface electrical resistivity tomography. *Water Res. Research.* 39(5): Article #1138.

Mills W.B., Liu M.C., Rigby M.C., Brenner D. 2007. Time variable simulation of soil vapor intrusion into a building with a combined crawl space and basement. *Env. Sci. and Technol.* (41): 4993-5001.

Moldrup P.T., Olesen J., Gamst P., Schjonning P., Yamguchi T., Rolston D.E. 2000. Predicting the gas diffusion coefficient in repacked soil: Water-induced linear reduction model. *Soil Sci. Soc. Am. J.* (64): 1588-1594.

Nazaroff W.W. 1998. Predicting the rate of 222Rn entry from soil into the basement of a dwelling due to pressure-driven air flow. *Radiation Protection Dosimetry.* 22(1-4): 199-202.

Olayinka Al. 1999. Advantage of two-dimensional geoelectrical imaging for groundwater prospecting: case study from Ira, southwestern Nigeria. *Water Res. J. Nig. Assoc. Hydrogeol.* (10): 103-113.

Oldenburg, D.W., and Li, Y. 1994. Inversion of Induced Polarization Data, *Geophysics.* (59): 1327-1341.

Olayinka Al., Yaramanci U. 1999. Choice of the best model in 2-D geoelectrical imaging: case study from a waste dump site. *Eu. J. Environ. Eng. Geophy.* 3: 221-244.

Ozcep F., Tezel O., Asci M. 2009. Correlation between electrical resistivity and soil-water content: Istanbul and Golcuk. *International Journal of Physical Sciences.* 4 (6): 362-365.

Patterson B.M., Davis G.B. 2009. Quantification of vapor intrusion pathways into a slab-on-ground building under varying environmental conditions. *Environ. Sci. Technol*. (43): 650-656

Pennell K.G., Bozkurt O., Suuberg E.M. 2009. Development and application of a 3-D finite element vapor intrusion model. *Journal of the Air and Waste Management Association*. In Press.

Sakaki, T., Limsuwat A., Smits. K., Tissa H. Illangasekare. 2008. Empirical two-point α-mixing model for calibrating ECH2O EC-5 soil moisture sensor in sands, *Water Resources Research*. (44): W00D08.

Sakaki, T., P. E. Schulte, A. Cihan, J. A. Christ and Tissa H. Illangasekare. 2011. (in revision), Airflow pathway dynamics in heterogeneous subsurface influenced by land surface boundary conditions, *Vadose Zone Journal*. 11-0118.

Schwartz B.F., Schreiber M.E., Yan T.T. 2008. Quantifying field-scale soil moisture using electrical resistivity imaging. *J. of Hydrology.* 362(3-4): 234-246.

Sheriff R.E. 2004. Encyclopedic Dictionary of Exploration Geophysics, *Geophysical Reference Series 1, Fourth Edition.*

Slater L., Binley A., Versteeg R., Cassiani G., Birken R., Sandberg S. 2002. A 3D ERT study of solute transport in a large experimental tank. *J. of App. Geophy*. (49): 211-229.

Smits K., Sakaki T., Limsuwat A., Illangasekare T.H. 2010. Thermal Conductivity of Sands under Varying Moisture and Porosity in Drainage-Wetting Cycles. *Vadose Zone Journal.* (1): 172-180.

Tillman F.D., Weaver J. W. 2007. Temporal moisture content variability beneath and external to a building and the potential effects on vapor intrusion risk assessment. *Science of the Total Environment*. 379 (1): 1-15.

[UBC GIF] University of British Columbia - Geophysical Inversion Facility. 2007. Vancouver, British Columbia

[USEPA] U.S. Environmental Protection Agency. 2008. Draft US EPA's vapor intrusion database: Preliminary evaluation of attenuation factors. Washington D.C.: USEPA Office of Solid Waste.

Yu S., Unger A., Parker B. 2009. Simulating the fate and transport of TCE from groundwater to indoor air. *J. of Cont. Hydro.* 107(3-4): 140-161.

APPENDIX A

ERT THEORY AND APPLICATION

A-1 ERT General Theory

The use of geoelectrical techniques to define subsurface structures dates back to the early twentieth century when Conrad Schlumberger conducted the first geoelectrical resistivity surveys in the fields of Normandy in 1912 [Kunetz, 1966]. Over the last century, geoelectrical resistivity survey techniques have improved significantly. As a result of these advances, geoelectrical resistivity techniques have become a critical instrument used in hydrogeological studies, mining exploration, engineering projects, and environmental investigations [*Griffiths et al.*, 1990; *Griffiths and Barker*, 1993; *Dahlin and Loke*, 1997; *Olayinka*, 1999; *Olayinka and Yaramanci*, 1999; *Amidu and Olayinka*, 2006; *Aizebeohai et al.*, 2010].

This study investigated a novel application of ERT to characterize VI pathway evolution by capturing relative moisture contents and lithologic profiles. ERT methods are based on the theory that electric fields caused by a current introduced into the ground can be observed and interpreted to represent the composition of the subsurface [*Sheriff*, 2004]. Resistivity is the property of a material that resists the flow of electrical current. The term is normally restricted to include only those methods in which a direct current, or very slowly oscillating current, is used to measure the apparent resistivity. As illustrated in **Figure A-1**, the basic components needed for an ERT survey are the electrodes used for the current induction (points A and B), the electrodes used for taking a voltage potential measurement (points M and N), and a current source.

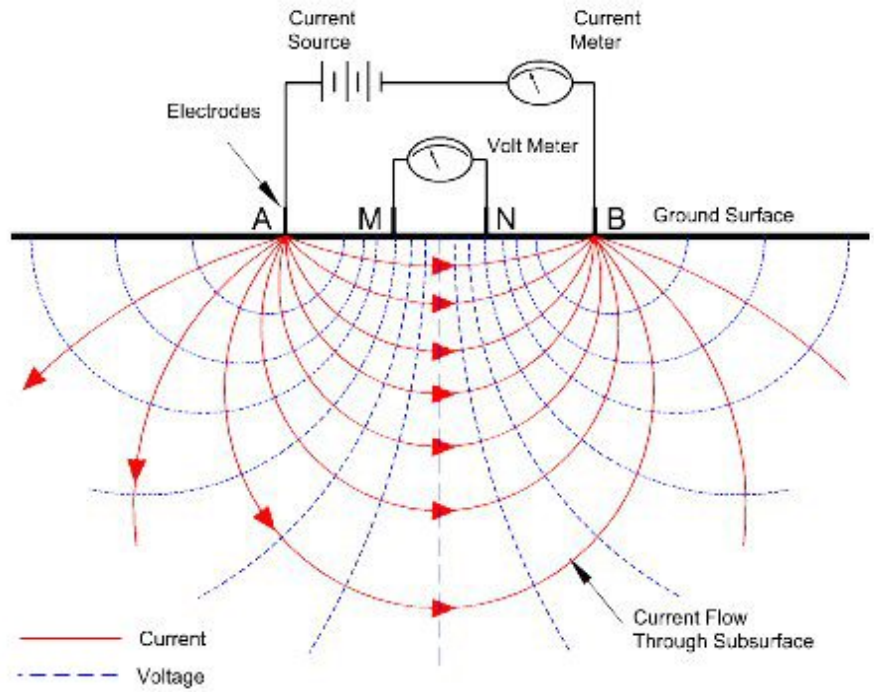

Figure A-1. Typical ERT Configuration [*Sheriff*, 2004].

The relationship between the current injected (I) and voltage observed (V) can be used to derive the apparent resistivity values (ρ_a) of the subsurface from Equation A-1:

$$\rho_a = k*V/I \qquad \text{(A-1)}$$

where k is a geometric factor that corresponds to the array configuration used during the survey. Most ERT equipment records voltage values in resistivity (R), where R = V/I, therefore the relationship between resistance and apparent resistivity is represented by

Equation A-2:

$$\rho a = k*R \qquad \text{(A-2)}$$

The observed apparent resistivity values do not represent the true geoelectrical composition of the subsurface; they represent values based on a homogenous composition. From these measurements, a true (non-unique) resistivity cross-section representing the heterogeneous composition of the subsurface can be estimated by processing the data through an inversion scheme. The inversions schemes currently used range from simple free-ware versions to complex and expensive proprietary software programs [*Dahlin and Loke*, 1997].

A-2 ERT Array Configurations – Advantages and Disadvantages

By rearranging the electrode array positions, several different types of electrode arrays can be constructed, each with distinct advantages and disadvantages. For field applications, the array chosen depends on several factors such as, the site subsurface heterogeneity, the types of structures being delineated, background noise levels, sensitivity to vertical or lateral delineations, depth of investigation required, spatial data coverage required, and signal strength of the array. *Dahlin and Loke* [1997] and *Aizebeokhai et al.* [2009] all have produced studies that thoroughly evaluate commonly used ERT array configurations. The following list highlights the advantages and disadvantages associated with the five most commonly used surface electrode array configurations.

(1) Wenner (alpha) array: This array utilizes two current electrodes and the two potential electrodes placed in-line with each other at equidistant distances from one another. Each measurement conducted using this array configuration is centered on a common location. Pros: This array is relatively sensitive to vertical variations in subsurface, especially below the center point of the array profile. This configuration has the ability to provide moderate depth of investigation and strong signal strength; which is necessary in environments with high levels of background noise. Cons: This array is less sensitive to horizontal variations in the subsurface and three-dimensional (3D) structures.

(2) Schlumberger: This array utilizes two current electrodes and the two potential electrodes placed in-line with one another and centered on a specific data point location. The unique aspect of this array configuration is that the potential and current electrodes are not placed equidistant from one another; instead, the current electrodes are placed much further from the center point location than the two potential electrodes. Pros: This array is relatively sensitive to vertical variations in subsurface resistivity below the center

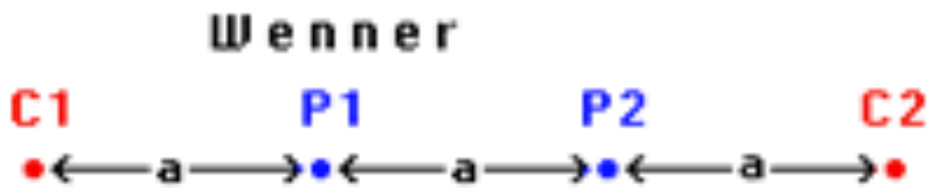

Figure A-2. Schematic of typical Wenner array configuration, with k = geometric factor, c = current source, p = potential electrode, a = electrode separation, n = an integer [*UBC GIF,* 2007].

of the array profile. This array can provide moderate depth of investigation and strong signal strength; which is necessary in environments with high levels of background noise. Cons: This array is less sensitive to horizontal variations in the subsurface and 3D structures.

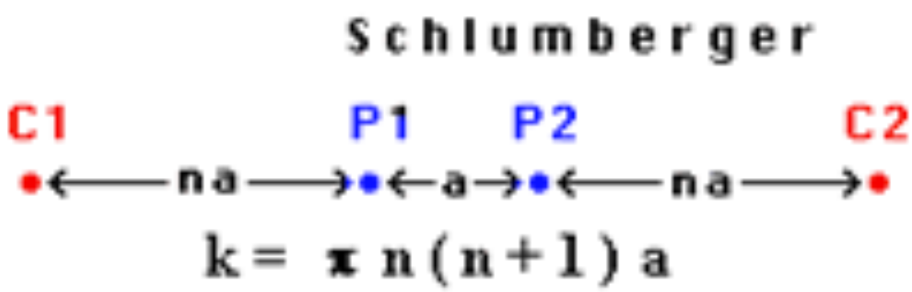

Figure A-3. Schematic of typical Schlumberger array configuration, with k = geometric factor, c = current source, p = potential electrode, a = electrode separation, n = an integer [*UBC GIF*, 2007].

(3) Dipole-Dipole: This array utilizes two current electrodes and two potential electrodes placed in pairs at opposite equidistant locations from a center data point location along the surface profile. Pros: This array configuration is very sensitive to resistivity variations below the electrodes in each dipole pair. This array configuration is also very sensitive to horizontal variations and 3D structures in the subsurface. Cons: This array configuration is less sensitive to vertical variations in the subsurface resistivities. The depth of investigation for this array depends on the current used and electrode spacing selected.

(4) Pole-Pole: This array configuration is constructed by simulating the second current electrode and the voltage potential electrode at infinite distances from the primary

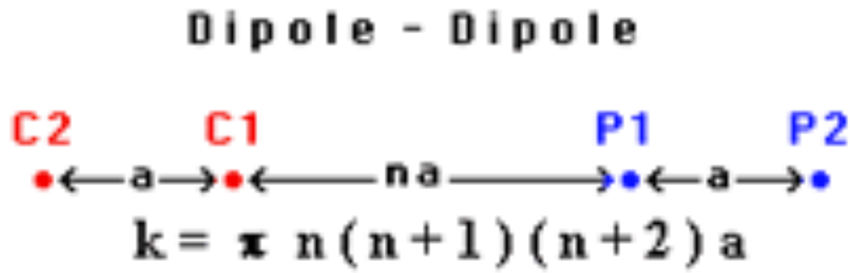

Figure A-4. Schematic of typical Dipole-Dipole array configuration, with k = geometric factor, c = current source, p = potential electrode, a = electrode separation, n = an integer [*UBC GIF*, 2007].

electrode set. Pros: This array configuration is the most effective for large area horizontalcoverage and deep investigations. Cons: This array configuration is highly sensitive to telluric noise capable of degrading the quality of data collected and the resolution. Due to poor resolution characteristics, subsurface structures to get smeared out in the inversion model processing stage.

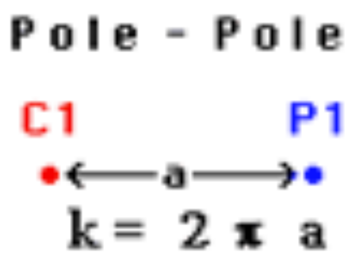

Figure A-5. Schematic of typical Pole-Pole array configuration, with k = geometric factor, c = current source, p = potential electrode, a = electrode separation, n = an integer [*UBC GIF*, 2007].

(5) Pole-Dipole: This is an asymmetrical array with asymmetrical apparent resistivity anomalies in the pseudo sections over a symmetrical structure, which often can influence the inversion model. Pros: This array configuration provides good horizontal coverage and relatively high signal strength. Cons: This array configuration is less sensitive to telluric noise than the pole-pole array. Studies have shown that repeating the measurements in the reverse order may eliminate the asymmetrical effect, however, this would significantly increase the required survey time and cost.

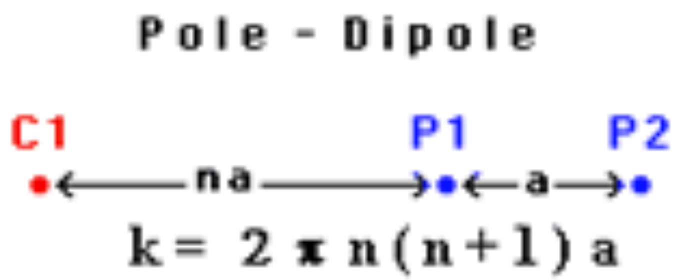

Figure A-6. Schematic of typical Pole-Dipole array configuration, with k = geometric factor, c = current source, p = potential electrode, a = electrode separation, n = an integer [*UBC GIF*, 2007].

A-3 Using ERT to Quantify Soil Moisture

Quantifying soil moisture distribution in the unsaturated zone has been extensively investigated. However, data is most commonly obtained through destructive sampling techniques, preventing the continuous measurement of transient conditions and providing no continuous data on soil moisture as a function of time. Destructive methods such as soil core extraction and field sampling have been shown to deviate from actual soil moisture properties [Liu, 2007]. This study will approach soil moisture characterization without the use on destructive sampling techniques.

Many studies over the past decade have demonstrated the performance of non-invasive ERT methods in characterizing moisture distribution profiles in the shallow subsurface [Michot et al., 2003; Swartz et al., 2008; Ozcep et al., 2009; Brunet et al., 2010; Franz et al., 2010). One of the most widely used relationships between soil resistivity and water content is *Archie's* relationship (1942). Several recent studies have demonstrated the application of Archie's relationship for characterization of soil water content in the unsaturated zone using ERT [*Schwartz et al.*, 2008; *Franz et al.,* 2010).

Archie's relationship is described by Equation A-3:

$$\rho = \rho_0 S^{-\beta} \qquad \text{(A-3)}$$

where S is the effective saturation, ρ is the resistivity of the porous medium, ρ_0 is the resistivity of the porous medium at full saturation, and β is a parameter related to the properties of the porous medium. The effective saturation is defined as $S = (\theta - \theta_r)/(\theta_s - \theta_r)$ where θ is the volumetric water content (cm^3/cm^3), and θ_s and θ_r are the saturated and residual volumetric water contents (cm^3/cm^3), respectively. By collecting soil samples at representative locations, the parameters used in Archie's relationship, θ_s, θ_r, and β, can be estimated by data fitting and laboratory analysis. Using Equation 3, the soil resistivity values captured by ERT, and the related parameters, θ_s, θ_r, β, and ρ_0, a two-dimensional (2D) soil moisture distribution of the subsurface can be estimated. Figure A-7 outlines the approach used in applying the *Archie* relationship to soil water content using ERT methods.

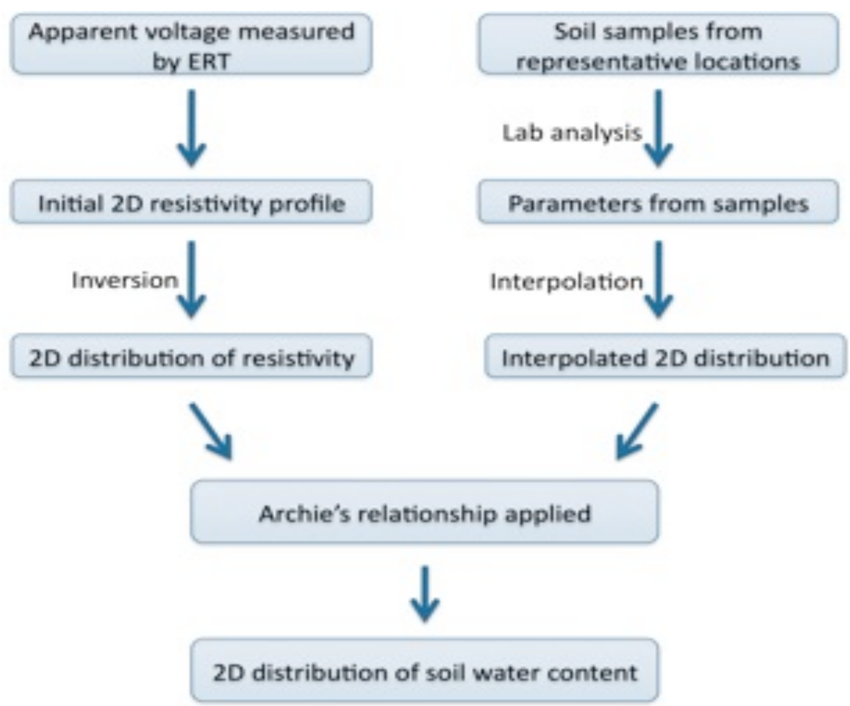

Figure A-7. Flow diagram for applying *Archie's* relationship to resistivity values.

APPENDIX B

PROJECT BACKGROUND

B-1 SERDP - Statement of Need

The funding for this project is based on Statement of Need (SON) released to the public in November of 2007 (SON Number: *ERSON-09-03*) by the Strategic Environmental Research and Defense Program (SERDP). The SON called for applied research in VI processes and characterization methodologies. Specifically, the SON outlined the need for a better understanding of VI pathways origination and evolution form chlorinated solvent-contaminated groundwater sources. The Center for Environmental Study of Subsurface Processes (CESEP) was rewarded a SERDP grant (SERDP Project: *ER-1687*) based on this SON to investigate fundamental processes that drive VI pathway evolution. All previous experimentation on this study was performed in the CESEP laboratory at the Colorado School of Mines.

B-2 SERDP Study at CESEP Overview

The research conducted during this study represents a small component of a larger multi-year SERDP-funded study on VI processes. SERDP granted the funding to the CESEP laboratory to conduct the following investigations:

(1) Study of vapor generation from NAPL sources in unsaturated zone with a fluctuating water table. This task was conducted at bench scale in a sand tank apparatus.

(2) Study of the effects of climate conditions on soil moisture variability in the unsaturated zone. This task was conducted at bench scale in a sand tank.

(3) Attenuation of vapors in the unsaturated zone. Specifically, this task focuses on integrating information about fundamental physical, chemical, and biological processes by developing a numerical model to quantify the relationships between these processes.

(4) Data generation using climate wind tunnel/porous media test facility. Specifically, an upscale and coupling of steps (1) and (2).
(5) Evaluation of existing modeling codes and development of a discussion-making toolbox for users.
(6) Determine and develop geophysical methods to rapidly and effectively characterize VI pathways. Initial tests from task (2) indicate that moisture distribution in the unsaturated zone plays a key role in the evolution of VI pathways. Based on these results, a geophysical method that has the capacity to capture moisture profiles was investigated during this phase of the study. This was accomplished through a series of intermediate-scale sand tank experiments.
(7) Upscale of geophysical sand tank experiments to perform field demonstrations of VI characterization methodology. This task was conducted at a Department of Defense (DoD) site with active VI processes occurring.

The research conducted in this thesis investigated be the geophysics portions, sections (6) and (7), of the SERDP study outlined above.

APPENDIX C

EQUIPMENT AND SENSORS USED DURING EXPERIMENTATION

C-1 ERT – Advanced Geosciences SuperSting R8 Earth Resistivity Meter

A SuperSting R8 IP 8-channel earth resistivity meter (Advanced Geosciences Inc., Austin, TX) with 28 stainless steel electrodes was used to perform the ERT surveys along surface profiles in the sand tank. The SuperSting R8 IP (seen in Figure C-1) earth resistivity meter is a multi-channel, portable device with internal memory and user defined measurement cycles. The meter provides the high accuracy and little noise. The meter has the capacity to simultaneously record up to 8 channels at once. In addition to the meter specifications, the main data cable contains several unique technological advances. The main data cable uses a patented multi-channel swift dual mode automatic multi-electrode design. This new patented design allows for much more efficient three-dimensional surveys. In addition, electrode address uses a 16-bit code allowing for up to 65,000 electrodes. The controlled to the resistivity is completely integrated into the main body of the unit and utilizes a high-powered transmitter, which can operate on both 12V and 24V battery systems.

C-2 Moisture Sensors – Decagon Devices Inc. EC-5 Sensor

Developing effective methods for obtaining soil moisture contents is critical for many environmental and hydrologic problems facing scientists today. Two of the most widely used methods include gravimetric and geophysical methods. Gravimetric methods calculate soil moisture values by using volumetric ratios of total mass of water to the total bulk mass of the soil sample. Geophysical methods, however, rely on observing the geoelectrical properties associated with the interaction between soil and water. Common geophysical methods include time-domain reflectometry (TDR), neutron probe, frequency domain sensor, capacitance probe, electrical resistivity tomography, ground penetrating radar (GPR) [*Ozcep et al.*, 2009].

Figure C-1. SuperSting R8 IP Earth Resistivity Meter (Advanced Geosciences Inc., Austin, TX, 2010).

Recent work performed by Sakaki et al. [2008] have shown that frequency domain type sensors can be calibrated to perform on par with TDR methods, at a fraction of the cost. The sensors used in this study were of the frequency domain type (ECH$_2$O EC-5, length = 5.5 cm, measurement frequency = 70 MHz, Decagon Devices, Inc., Pullman, WA) (*Decagon Devices*, 2006), seen in Figure C-2. This type sensor design relies on taking measurements of the dielectric constant of the soil matrix surrounding the sensor. See Table C-1 for full list of manufacturer's specifications associated with this sensor design.

Several steps are necessary to convert the raw digital signals produced by the ECH$_2$O EC-5 sensor into moisture content values. The ECH$_2$O EC-5 sensor first produces a raw signal in the mV range, which our data logger (Em50 data logger or

ECH_2O EC-5 check hand-held reader, 12-bit, excitation voltage = 3V, Decagon Devices, Inc., Pullman, WA) automatically converts into an analog-to-digital converter number

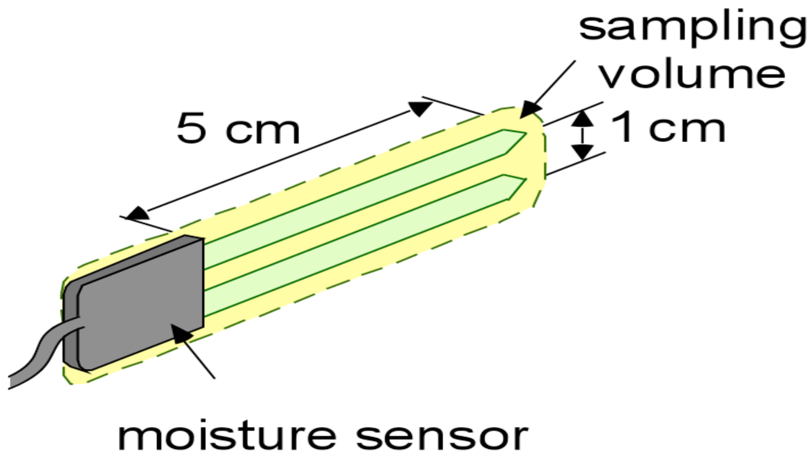

Figure C-2. Schematic of ECH_2O EC-5 soil moisture sensor and sampling volume (Decagon Devices Inc., Pullman, MO).

Table C-1. ECH_2O EC-5 soil moisture sensor specifications.

ECH_2O EC-5 Soil Moisture Sensor Manufacturer's Specifications[1]:	
Accuracy	Mineral Soil: ±3% VWC, most mineral soils, up to 8 dS/m ±1-2% VWC with soil specific calibration Rockwool: ±3% VWC, 0.5 to 8 dS/m Potting Soil: ±3% VWC, 3 to 14 dS/m
Resolution	0.1% VWC (mineral soil) 0.25% VWC (rockwool)
Range	calibration dependant; up to 0-100% VWC with polynomial equation
Dimensions	8.9 x 1.8 x 0.7 cm
Cable Length	5 m, custom cable lengths available upon request
Measurement Time	10 ms
Power	2.5 - 3.6 V DC @ 10 mA. Output proportional to input voltage. 2.5 V and 3 V excitations supported with calibration equations
Output	Voltage, correlated linearly (soil) or polynomially (growing media) with VWC
Temperature	-40°C to +50°C
Connector Types	3.5 mm "stereo" plug or stripped and tinned lead wires (3)
Datalogger Compatibility	Decagon: Em50, Em50R, ProCheck, ECH2O Check, Em5b Campbell Scientific: CR10X, 21X, 23X, CR1000, CR3000, etc. Other: Any data acquisition system capable of switched 2.5 to 3.6 V excitation and single ended voltage measurement at 12 bit or better resolution.
Warrenty	One year, parts and labor

[1] 2012 Decagon Devices, Inc., EC-5 Soil Moisture Website Database

(ADC). The ADC number is then converted to soil moisture content values by incorporating the non-linear relationship developed by *Sakaki et al.* [2008]. This process is essentially a two-step field/laboratory calibration procedure; step one involves obtaining an ADC reading in totally dry sands and step two involves obtaining an ADC in completely saturated sands. Once these two values are collected, the non-linear relationship shown in Equation 5.1 can be applied.

In addition to the calibration methods developed through the observational studies performed by *Sakaki et al.* [2008], several other experiments performed in our laboratory have successfully demonstrated the accuracy of utilizing this non-linear relationship between ADC values and soil moisture contents. Figure C-1 shows a schematic of the ECH_2O EC-5 soil moisture sensor as well as its sampling volume.

C-3 Temperature Sensors – Decagon Devices ECT Sensor

The soil temperatures for all experiments were recorded using a simple thermistor type, ECT soil/air temperature sensor manufactured by Decagon Devices Inc. (Decagon Devices, Inc., Pullman, WA). The ECT sensor is completely water proof, submersible, and designed for continuous indoor/outdoor use. See Table C-2 for complete list of manufacturer's specifications. During laboratory sand tank experimentation, as well as during field demonstrations, soil temperature readings were obtained using the ECT soil moisture sensor and logged with a compatible data logger (Em50 data logger, Decagon Devices, Inc., Pullman, WA).

Table C-2. ECT soil temperature sensor specifications.

ECT Soil Temperature Sensor Specifications[1]:	
TEMPERATURE ACCURACY	- 40 to -20°C: ±1.0°C 5 to 40°C: ±0.5°C 40 to 50°C and -20 to 5°C: better than ±1.0°C
TEMPERATURE RESOLUTION	0.1°C
TEMPERATURE RANGE	- 40°C to 50°C
MEASUREMENT SPEED	8.9 x 1.8 x 0.7 cm
CABLE LENGTH	5 m, custom cable lengths available upon request
MEASUREMENT SPEED	10 mS
SENSOR TYPE	Thermistor
OUTPUT	320-1000mV @ 3V excitation
OPERATIING ENVIRONMENT	-40°C to +50°C
POWER	2.5VDC @ 2mA, to 3.6VDC @ 7mA
CABLE LENGTH	3m
CABLE CONNECTOR TYPES	3.5mm "stereo" plug or stripped and tinned lead wires (3)
SENSOR DIMENSIONS	11.2cm x5.8cm x.075cm
DATA LOGGER COMPATIBILITY	Decagon: Em5B, Em50, Em50R, ProCheck, Campbell Scientific: CR10X, 21X, 23X, CR1000, CR3000, etc. Other: Any data acquisition system capable of 3-15VDC excitation and single ended voltage measurement at 12 bit or better resolution
WARRANTY	One year, parts and labor

[1] 2012 Decagon Devices, Inc., ECT soil temperature online database